Nitroimidazopyrazinones with oral activity against tuberculosis and Chagas disease in mouse models of infection

Chee Wei Ang[1,2*], Brendon M. Lee[3,4], Colin J. Jackson[3], Yuehong Wang[5], Scott G. Franzblau[5], Amanda F. Francisco[6], John M. Kelly[6], Paul V. Bernhardt[7], Lendl Tan[7], Nicholas P. West[7], Melissa L. Sykes[8], Alexandra O. Hinton[1], Raghu Bolisetti[1], Vicky M. Avery[8,9], Matthew A. Cooper[1], Mark A.T. Blaskovich[1,*]

[1] Center for Superbug Solutions, Institute for Molecular Bioscience, The University of Queensland, St Lucia, Queensland 4072, Australia

[2] School of Science, Monash University Malaysia, Subang Jaya, 47500 Selangor, Malaysia

[3] Research School of Chemistry, Australian National University, Sullivans Creek Road, Acton, ACT 2601 Australia

[4] Division of Infectious Diseases, Department of Medicine, Weill Cornell Medical College, New York, NY 10021, USA

[5] Institute for Tuberculosis Research, College of Pharmacy, University of Illinois at Chicago, Chicago, Illinois 60612, USA

[6] Department of Infection Biology, London School of Hygiene & Tropical Medicine, Keppel Street, London WC1E 7HT, United Kingdom

[7] School of Chemistry and Molecular Bioscience, The University of Queensland, St Lucia, Queensland 4072, Australia

[8] Discovery Biology, Griffith Institute for Drug Discovery, Griffith University, Don Young Road, Nathan, Queensland 4111, Australia

[9] School of Environment and Science, Griffith University, Nathan, Queensland 4111, Australia

Abstract

Tuberculosis and parasitic infections continue to impose a significant threat to global public health and economic growth. There is an urgent need to develop new treatments to combat these diseases. Here, we report the *in vitro* and *in vivo* profiles of a new bicyclic nitroimidazole subclass, namely nitroimidazopyrazinones, against mycobacteria and *Trypanosoma cruzi*. Derivatives with monocyclic side chains were selective against *Mycobacterium tuberculosis*, and were able to reduce the bacterial load when dosed orally in mice. We demonstrated that deazaflavin-dependent nitroreductase (Ddn) could act effectively on nitroimidazopyrazinones, indicating the potential of Ddn as an activating enzyme for these new compounds in *M. tuberculosis*. Oral administration of compounds with extended biaryl side chains (**73** and **74**) was effective in suppressing infection in an acute *T. cruzi* infected murine model. These findings demonstrate that active nitroimidazopyrazinones have potential to be developed as orally available clinical candidates against both tuberculosis and Chagas disease.

Introduction

Tuberculosis (TB) is one of the world's deadliest infectious diseases. It is caused by *Mycobacterium tuberculosis*, a slow growing bacterial pathogen that was discovered by Dr. Robert Koch in 1882. According to the World Health Organization (WHO), it was estimated that 10 million people developed TB in 2020, with a death toll of 1.5 million.[1] In most cases, TB is treatable with a standard 6-month drug

regimen comprised of isoniazid, rifampicin, ethambutol and pyrazinamide.[1] However, with the inexorable increase in drug resistance over the past decades, many first-line or even second-line antitubercular agents are no longer effective. It was reported that treatment success rates for rifampicin-resistant or multidrug-resistant TB were 55–59% in 2015-2018, compared to an average of 85% for drug-susceptible TB.[1] Following the theme of World TB Day 2021 - 'The Clock is Ticking', there is a pressing need to find new treatment options to end this old millennium disease. Given that current treatment regimens are long and complicated, which then lead to poor patient compliance, the desired target product profiles (TPPs) of new TB drugs focus on shortening the treatment duration, reducing the dosing frequency, enabling easy administration (ideally once a day oral dosing), and having the ability to overcome drug-resistant strains.[2, 3]

Alongside TB and other more commonly known infectious diseases such as human immunodeficiency virus (HIV) and malaria, neglected tropical diseases (NTDs) are known as 'infectious diseases of poverty' as they affect the world's poorest population.[4] Chagas diseases (CD), or American trypanosomiasis, affects 6–7 million people worldwide and causes a huge annual economic loss of $7.2 billion.[5, 6] It is caused by the trypanosomatid parasite *Trypanosoma cruzi* that is transmitted mainly through a triatomine bug known as 'kissing bug'.[7] Although CD primarily affects Latin American countries, in recent years it has become a health concern for other continents including Europe, North America, and Australia due to population migration.[6, 8] Current therapeutic options for CD are limited to benznidazole **1** and nifurtimox, drugs that were discovered in the 1960s and1970s. However, they suffer from various adverse effects, require long treatment duration, and have dubious efficacy in chronic infections.[9] Hence, ideal TPPs focus on new regimens that have a shorter treatment course, are safe and more efficacious than current drugs, exhibit good oral bioavailability, and are active against both chronic and acute phases.[10] New drugs should also achieve total clearance of parasites in patients to prevent relapse after treatment.[11] In recent years, combination therapies that utilize multiple drugs with different

mechanisms of action have been found to be effective in preclinical testing.[12, 13] Whilst combinations have been tested in clinical trials, their efficacy compared to individual drug components alone have yet to be identified.[13]

There are many challenges in the area of TB and CD drug discovery. In the case of TB, hits identified through target-based screening almost always fail to show sufficient or comparable whole-cell activity. One of the reasons is due to the waxy, lipid-rich mycobacterial cell wall with low permeability, preventing most potential antibiotics from passing through and reaching the intracellular molecular targets.[14] In addition, efflux systems extrude a range of substrates, including drugs, out of the cells. In contrast, for *T. cruzi* there is lack of well-validated targets, thus most drug discovery efforts focus on phenotypic screening, providing cell permeable hits.[15] Fexinidazole **2** was "re-discovered" by the Drugs for Neglected Diseases *initiative* (DND*i*) using phenotypic-based assays, and **2** was ultimately evaluated as a clinical candidate for both human African trypanosomiasis (HAT) and CD.[16, 17] Two of the most recently approved TB drugs, delamanid **3** and pretomanid **4**, were also identified using phenotypic approaches.[18] They were later found to have repurposing potential against visceral leishmaniasis (VL),[19, 20] which is caused by the kinetoplastid protozoan, *Leishmania*. Through a collaborative program between the University of Auckland, TB Alliance, and DND*i*, a backup library of 900 analogs of **4** have been counter-screened against *Trypanosoma brucei* and *T. cruzi,* resulting in the discovery of several promising hits to be pursued.[21, 22]

Benznidazole **1**, fexinidazole **2**, delamanid **3**, and pretomanid **4** (Figure 1) all belong to the nitroimidazole family of drugs, which has a long history of use as treatments against bacterial and parasitic infections.[23] They are prodrugs that require bioactivation of the nitro group to exert their antimicrobial activity. The bicyclic nitroimidazole drugs, **3** and **4** are active against both actively growing and non-replicating mycobacteria, making them an ideal candidate to shorten treatment duration.[24] They have interesting multiple modes of action. Under aerobic condition, these compounds target the mycobacterial cell wall

by inhibiting the biosynthesis of mycolic acid.[25] When mycobacteria are in a hypoxic, non-replicating state, they cause respiratory poisoning by releasing nitric oxide (NO) intracellularly through bioactivation of the nitro group.[26] It has recently been found that a protein encoded Rv3547 is responsible for the reductive activation of **3** and **4** in *M. tuberculosis*.[27, 28] This enzyme is now known as deazaflavin-dependent nitroreductase (Ddn).[29] The Ddn mediated metabolism of **4** produced three stable metabolites, and one of the major products is a des-nitro species, which correlates well with the release of NO and its anaerobic bactericidal activity.[26] Reduction of **3** by Ddn generated adducts with NAD^+ in *M. tuberculosis*, suggesting its potential importance in the action of **3** under both normoxic and hypoxic conditions.[30] However, the Ddn enzyme is absent in kinetoplastids such as *T. cruzi* and *Leishmania*. It has recently been found that bicyclic nitroimidazoles are activated by a novel nitroreductase (NTR2) in *Leishmania*.[31] The NTR2 *Leishmania* enzyme could not activate the monocyclic nitroimidazole **2**, which instead was mediated by a type I nitroreductase (NTR1).[32] Although the metabolic fate of **2** in *T. b. brucei* and *T. cruzi* remains unknown, diminished NTR1 activity resulted in resistance to **2** and cross-resistance to other nitroaromatic drugs including nifurtimox.[33] This suggests that there are diverse modes of action of nitroimidazoles between different organisms.

We have previously described the synthesis of two novel regioisomeric bicyclic nitroimidazole scaffolds, the nitroimidazopyrazinones **5** and the nitroimidazopyrazines **6** (Figure 1). The nitroimidazopyrazinones **5** in particular possessed antitubercular activity under both aerobic and hypoxic conditions (MIC = 0.06–32 μg/mL).[34] Several promising hits were found to have comparable or better *in vitro* activity than **4**, while displaying low cytotoxicity against mammalian cell lines, good metabolic stability and high Caco-2 permeability. The *in vitro* activity profile of **5** led to the current study, in which further evaluation of safety, efficacy and pharmacokinetic properties of this scaffold in murine models for both Chagas disease and tuberculosis have been undertaken. To expand the subclasses of bicyclic nitroimidazoles, new nitroimidazo-imidazolone/-pyrimidinone scaffolds with modifications on the pyrazinone component

were synthesized. Our earlier investigations revealed the importance of the nitro group in **5** for antimicrobial activity, as the des-nitro analogs were as inactive as des-nitro **4** against *M. tuberculosis*.[35] Considering the correlation between the electrochemical reactions at the interface of electrode-electrolyte and the enzymatic redox reaction,[36] we also now report the redox behavior of nitroimidazopyrazinones and their related subclasses using cyclic voltammetry (CV). To understand the possible modes of action of these new compounds against *M. tuberculosis*, we investigated whether they are activated by the same enzyme as **3** by conducting a biochemistry study using purified Ddn that is overexpressed in *Escherichia coli*. Lastly, we have explored the potential of selected nitroimidazopyrazinones in treating *T. cruzi* infection *in vivo*. Our previous *in vitro* results showed that the extended biaryl series could inhibit *T. cruzi* intracellular amastigotes, with IC_{50} values of ≤0.1 μM.[37] Here, we report the *in vivo* profile of two lead compounds against *T. cruzi*, compared to the existing drug, benznidazole **1**.

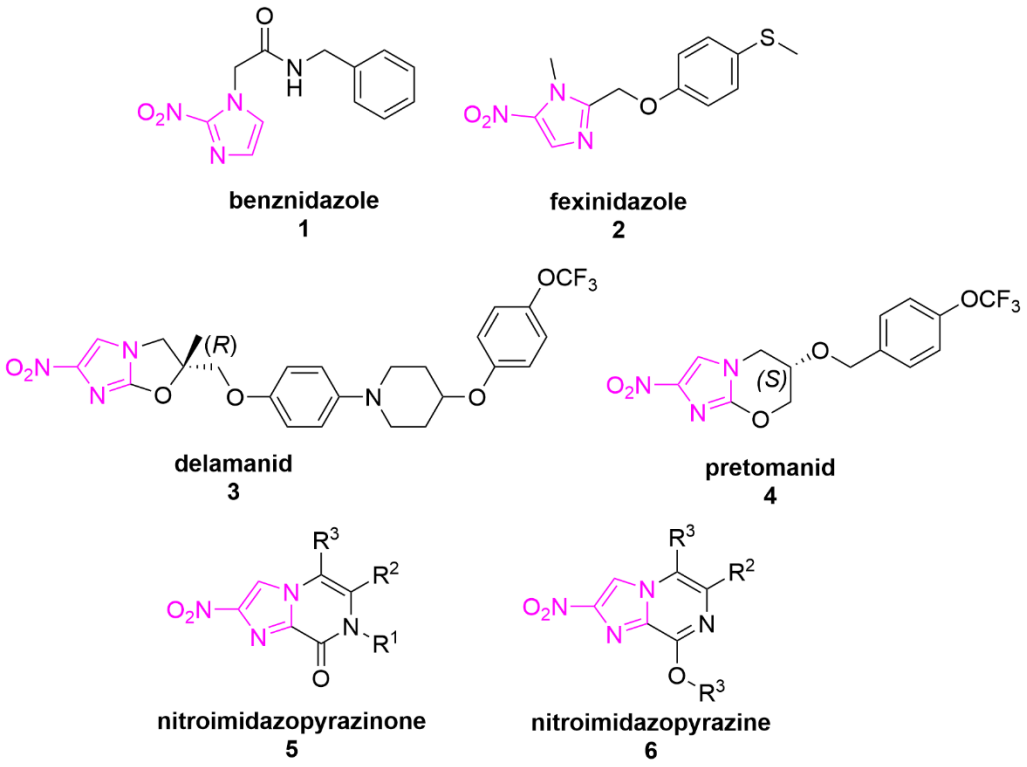

Figure 1. Chemical structures of monocyclic and bicyclic nitroimidazoles with antitubercular and/or antitrypanosomal activity.

Results and discussion

Antimycobacterial activity of nitroimidazopyrazinones

In our previous studies, a library of 71 nitroimidazopyrazinones **7–77** and 13 of their *O*-alkylated regioisomers, nitroimidazopyrazines **78–90** were synthesized (structures shown in Supporting Information Figure S1 and S2) and tested for their activity against *M. tuberculosis* H37Rv strain using a resazurin reduction assay.[34, 37] Given the encouraging activity demonstrated by the monocyclic side chain of pyrazinone under both normoxic and hypoxic conditions, additional *in vitro* susceptibility testing was performed to investigate their selectivity in different mycobacterial species (Table 1). Although *Mycobacterium smegmatis* has been used as a model system in most phenotypic screenings[38, 39] and its orthologs share 70% identity with *M. tuberculosis* genomes,[40] our compounds displayed no activity against this non-pathogenic strain, highlighting the dangers of screening with a surrogate organism. They were also non-active against the opportunistic pathogen *Mycobacterium avium* when tested at concentrations up to 32 μg/mL under normoxic condition. These results were similar to **4**, suggesting the potential of these molecules as selective chemical starting points for development of therapeutics for diseases caused by *M. tuberculosis* complex but not against the nontuberculous mycobacteria. Previous studies have shown that Ddn orthologues, including those from *M. smegmatis* and *M. avium*, are inactive against **4** due to differences in sequence identity.[41] This could also explain the lack of activity of pyrazinone derivatives in these mycobacteria when tested under normoxic condition.

Table 1. Minimum inhibitory concentrations (MICs) of nitroimidazopyrazin-one/-e derivatives against different mycobacterial species.

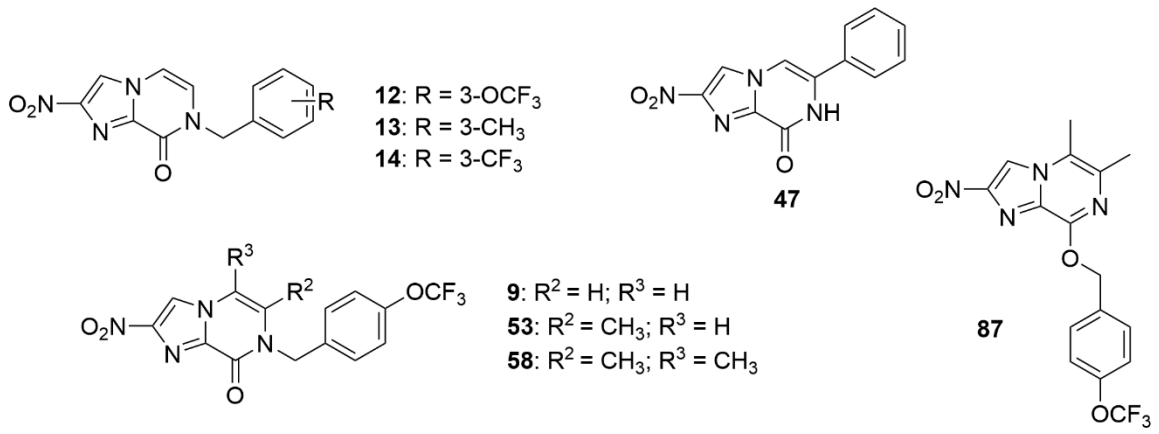

Compound	Antibacterial MIC (μg/mL) normoxic				Antibacterial MIC (μg/mL) hypoxic
	***M. tuberculosis* H37Rv**	***M. tuberculosis* H37Ra**	***M. avium***	***M. smegmatis***	***M. tuberculosis* (H37Rv)**
Pretomanid 4	0.25-0.50	≤0.016-0.063	>32	>32	1
9	0.5	0.031-0.25	>32	>32	1-4
12	0.13	0.13-0.25	>32	>32	0.5-2
13	0.063	≤0.016	>32	>32	70-90% I @ 0.125-8 μg/mL
14	0.063	≤0.016-0.031	>32	>32	0.25
47	>32	>32	>32	>32	>32
53	>32	4-8	>32	>32	>32
58	1	0.5	>32	>32	4
87	>32	>32	>32	>32	>32

Isoniazid control (normoxic): *Mtb* H37Rv MIC = 0.016 μg/mL, *Mtb* H37Ra MIC = 0.031-0.063 μg/mL, *M. avium* MIC = >32 μg/mL, *M. smegmatis* MIC = >32 μg/mL. Isoniazid control (hypoxic): *Mtb* H37Rv MIC = >5 μg/mL. Rifampicin control: *Mtb* H37Rv MIC = 0.005-0.01 μg/mL, *Mtb* H37Ra MIC = <0.016 μg/mL, *M. avium* MIC = 4 μg/mL, *M. smegmatis* MIC = 4 μg/mL. Rifampicin control (hypoxic): *Mtb* H37Rv MIC = 0.08-0.17 μg/mL.

To determine whether nitroimidazopyrazin-ones/-es have similar activity against both virulent and avirulent organisms, we have compared their bioactivity against *M. tuberculosis* H37Rv and H37Ra strains under normoxic condition. Both strains are derived from the parent strain H37, but with some differences at their genomic and proteomic levels.[42, 43] It was reported that H37Ra acquired multiple mutations in genes that might be associated with its virulence attenuation.[43, 44] In our study, H37Ra was more susceptible to the tested analogs, with ~2–16-fold better activity compared to its virulent counterpart. Compounds **13** and **14** remained the most activity against both strains, with MICs of ≤0.016–0.031 μg/mL against H37Ra and 0.06 μg/mL against H37Rv under normoxic condition. When tested

under low oxygen environment (0.1% oxygen), **14** surpassed the activity of pretomanid **4** against H37Rv (**14**: MIC = 0.25 μg/mL cf. **4**: MIC = 1 μg/mL). Activity against *M. tuberculosis* was only found for the pyrazinone scaffold, as the regioisomer nitroimidazopyrazine **87** completely lost potency under both normoxic and hypoxic conditions. A similar structure-activity relationship (SAR) was observed between the two *M. tuberculosis* strains, where addition of substituents at R^2 and R^3 resulted in loss of activity against H37Rv and H37Ra strains. These results indicate that the less-hazardous H37Ra strain can potentially be used as a surrogate for the virulent *Mtb* H37Rv to screen for potential antitubercular hits, though most of the analogs tested generally demonstrated better activity against this avirulent model. However, this would need to be further validated under hypoxic condition, in addition to confirming with a broader range of compounds and drugs. As H37Ra can be handled in a biosafety level II environment, it would be advantageous to use this strain instead of *M. smegmatis* for primary screening, with promising hits then subjected to a more rigorous MIC determination using the pathogenic H37Rv strain, which requires level III containment.

Electrochemical properties of nitroimidazopyrazin-one/-e scaffolds

We reasoned that the redox biochemistry of the nitro group is essential in mediating the biological activity of nitroimidazoles.[45] Pretomanid **4** exhibits antitubercular activity through the loss of the nitro group, which in turn generates reactive nitrogen species within the mycobacterial cells to achieve anaerobic bactericidal activity.[26] However, the nitroimidazole redox potential should be optimum to exhibit high specificity against target organisms without causing unnecessary toxic effects to the hosts. For example, metronidazole possesses a more negative redox potential that exceeds the reduction capacity of mammalian redox systems and aerobic microbes, making it selective against anaerobes such as non-replicating, hypoxic *M. tuberculosis.*[24] 2-Nitroimidazoles, on the other hand, have a higher redox potential and are therefore more readily reduced by mammalian cells, making them more suitable as

agents for cancer therapy.[46] One of the factors that affects the ease of nitro reduction is the electron affinity of the nitroheterocycles. As modification of molecular structure can affect the electrochemical properties and reduction potential of nitroimidazoles, the formal potentials (E′) of structurally related nitroimidazopyrazin-ones/-es were measured and compared using cyclic voltammetry (CV).

Initial measurements were undertaken in anhydrous DMSO as the reduction of nitroimidazoles is likely to be reversible under this condition, uncomplicated by coupled proton transfer. The E′ values were determined from the potential midway between the reduction and oxidation peaks, and calibrated against ferrocene. The peak-to-peak separation (> 59 mV and dependent on scan rate) was consistent with a quasi-reversible single electron transfer reaction to give the nitro radical anion as the product of electrochemical reduction. Metronidazole demonstrated a higher E′ than **4** (~200 mV difference, -1586 mV vs -1795 mV), which correlated well with a literature study.[36] The response for **4** was asymmetric ($i_{pc} > i_{pa}$ at 200 mV/s) with an additional peak found upon re-oxidation at higher potential (Supporting Information, Figure S3). Examination of the redox potentials of seven nitroimidazopyrazinones revealed a more positive E′ compared to **4**, with a range of -1555 to -1662 mV (Table 2). Compound **9** displayed the highest potential (-1555 mV). The similarity of voltammograms exhibited by both **9** and metronidazole indicated common electrochemical behavior. The addition of an electron-donating alkyl group at R^2 and R^3 (compound **58**) slightly increased the electron density of the nitroimidazole ring and consequently lowered its redox potential (-1566 mV). Pyrazine analog **87** is a regioisomer of **58** and showed an E′ value that was 30 mV more positive (-1536 mV). This also correlated well with the ^{1}H NMR analysis, in which the methylene protons (–O–CH_2–) of **87** showed a higher chemical shift (more deshielded) than **58** (–N–CH_2–).[34] Compound **47** had the lowest E′ among the series of nitroimidazopyrazinones (-1662 mV). However, there was no direct correlation between the whole cell antitubercular activity and the ease of reduction of nitroimidazoles in our case (Figure 2a), suggesting that factors other than redox activation are more crucial in determining their biological potential. As *M.*

tuberculosis has complex, multi-layer cell wall system, compound permeability could be the key that contributes to its antimycobacterial activity.[14]

As bioreduction of nitroimidazoles happens in an aqueous environment, the redox potential was further examined in a mixed medium, DMSO/PBS (70/30, v/v) with 0.1 M KCl as supporting electrolyte. However, the electrochemical reduction was irreversible due to the instability of radical anions in water in the presence of protons (data not shown). Multi-electron and proton associated irreversible reduction of nitro groups to give nitroso and hydroxylamine derivatives in aqueous solution is well established.[47] The lack of any reoxidation currents made reliable estimations of the redox potentials in aqueous solution problematic.

Ddn enzymatic activity

It is known that the F_{420}-dependent nitroreductase Ddn is responsible for the bioactivation of delamanid **3** and pretomanid **4** in *M. tuberculosis*.[28, 29] To investigate whether Ddn takes part in the activation of nitroimidazopyazinones, we first examined the efficiency of the most promising hit, **14** as a substrate of this enzyme. We determined the kinetic activity of Ddn reducing **4** by following the oxidation of reduced F_{420}, $F_{420}H_2$. We observed a K_M for **4** of 7.3 μM, a k_{cat} of 9.3×10^{-3} s^{-1} and k_{cat}/K_M of 1260 $M^{-1}s^{-1}$. This is similar to previously reported kinetic parameters of Ddn with **4**.[48] Compound **14** displayed a K_M of 9.4 μM indicating favorable binding with Ddn with a k_{cat} of 1.6×10^{-2}. Its k_{cat}/K_M of 1650 M^{-1} s^{-1} suggests that it is possibly a better substrate than **4**. To better understand the relationship between chemical structure and substrate efficiency, the kinetic parameters of structurally related analogs were explored (Table 2). The monocyclic nitroimidazole carboxamide **91** was a poor substrate for Ddn, consistent with the inability of Ddn to oxidize $F_{420}H_2$ when metronidazole was used as substrate.[48] Compounds **9** and **10** were similar to **14**, with a k_{cat}/K_M of 1640–1710 M^{-1} s^{-1}. However, when the trifluoromethoxy substituent was changed from a *para*- (**9**) to *meta*- (**12**) position, the binding affinity was reduced significantly from

2 μM to 45 μM, though antimycobacterial activity generally increased. The pyrazine analog **87** and its pyrazinone counterpart **58** shared similar K_M values (30 μM and 28 μM respectively), although the k_{cat} of **58** (6.9×10^{-3} s^{-1}) was ten-fold higher than **87** (7.0×10^{-4} s^{-1}). There was no correlation between Ddn substrate specificity and the ease of reduction as determined from CV. However, in most of the cases (except **12**), their activity as substrates was quite closely associated with the whole cell potency against *M. tuberculosis* (Pearson's r coefficient, r = -0.828, $p = 0.011$), indicating the potential importance of the Ddn enzyme in their activation (Figure 2b).

Table 2. Characterization of Ddn activity and electrochemical properties of nitroimidazopyrazin-ones/-es.

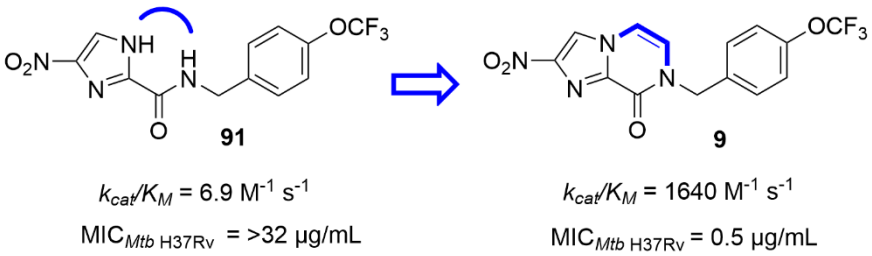

Compound	Core	R^1	R^2	R^3	k_{cat} (s^{-1})	K_M (μM)	k_{cat}/K_M (M^{-1} s^{-1})	E′ (mV) vs Fc[e]
Metronidazole					ns*	ns*	ns*	-1586
Pretomanid 4	-	-	-	-	$9.3\times10^{-3} \pm 4.8\times10^{-4}$	7.3 ± 1.4	1260	-1795
91	-	-	-	-	$2.1\times10^{-4} \pm 1.0\times10^{-5}$	31 ± 4.9	6.9	ND
47	A	H	Ph	H	$1.3\times10^{-3} \pm 9.8\times10^{-5}$	164 ± 36	8.1	-1662
9		4-OCF_3-benzyl	H	H	$3.3\times10^{-3} \pm 1.4\times10^{-4}$	2.0 ± 0.41	1640	-1555
10		4-CH_3-benzyl			$4.3\times10^{-3} \pm 2.9\times10^{-4}$	2.5 ± 0.52	1710	ND
12		3-OCF_3-benzyl			$3.1\times10^{-3} \pm 2.3\times10^{-4}$	45 ± 13	70	ND
14		3-CF_3-benzyl			$1.6\times10^{-2} \pm 6.5\times10^{-4}$	9.4 ± 1.3	1650	ND
53		4-OCF_3-benzyl	CH_3	H	ND	ND	ND	-1562
58		4-OCF_3-benzyl	CH_3	CH_3	$6.9\times10^{-3} \pm 7.2\times10^{-4}$	28 ± 8.1	244	-1566
87	B	4-OCF_3-benzyl			$7.0\times10^{-4} \pm 6.4\times10^{-5}$	30 ± 6.8	24	-1536

ns – not substrate; *results obtained from literature [48]; ND – not determined. Core A and B represents imidazopyrazinone and imidazopyrazine scaffold.

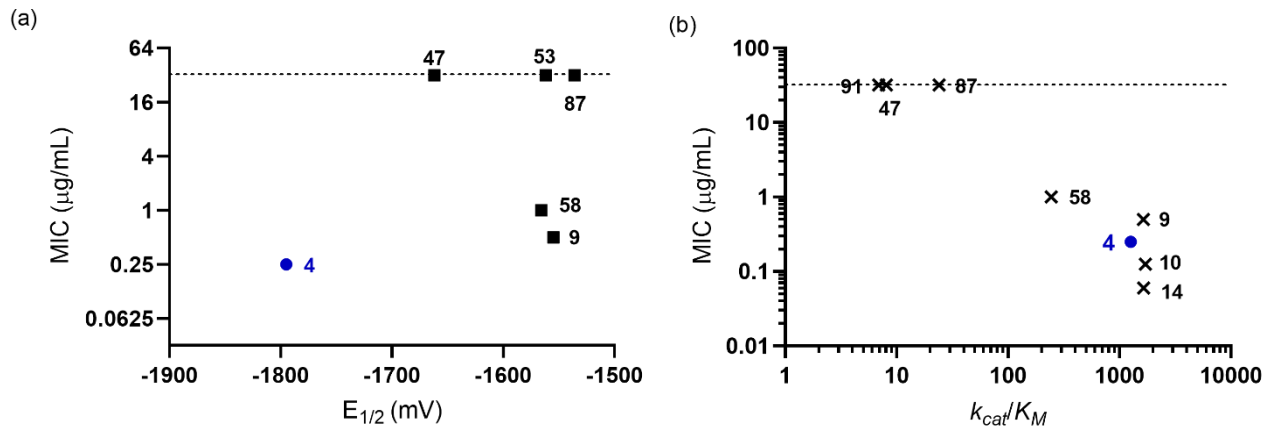

Figure 2. Correlation between the whole cell antitubercular activity (expressed as a log scale) and (a) redox potential (r = -0.291, R^2 = 0.085, p = 0.634); (b) catalytic efficiency as Ddn substrates (r = -0.828, R^2 = 0.686, p = 0.011). Dashed line represents the highest concentration tested (32 μg/mL) in minimum inhibitory concentration (MIC) assay.

Previous studies have suggested that the extended side chains of **4** are favorable to accommodate the binding pocket of Ddn which is rather linear and elongated.[49-51] Therefore, a second generation of nitroimidazopyrazinones was generated to explore the role of the biaryl side chains in binding to the hydrophobic pocket of Ddn.[37] We tested selected analogs for their kinetic activity with Ddn and the results are summarized in Table 3. The biphenyl compound **65** was found to have a stronger affinity (8.4 μM) and higher k_{cat}/K_M (370 M^{-1} s^{-1}) than the monoaryl **12** (45 μM, 70 M^{-1} s^{-1}), but this did not translate into having a lower MIC against *M. tuberculosis* (2 μg/ml and 0.125 μg/ml respectively). Replacement of one of the phenyl groups with a less lipophilic pyridine (**69**) or piperidine ring (**75**) resulted in marginal effects on both substrate specificity and cellular potency (5 μM and 4 μg/ml, 2.2 μM and 1-2 μg/ml respectively), with ~1–2-fold activity difference. Disrupting the molecular linearity and planarity of the extended side chains significantly improved the k_{cat}/K_m value, with the 3'-linked phenylpyridine (**72**) showing 12-fold better activity (3190 M^{-1} s^{-1}) compared to its linear 4'-linked counterpart **69** (266 M^{-1} s^{-}

[1]). It is postulated that this orientation may be preferred over the linear side chains for favorable interactions with the active site of Ddn. Compound **70** was the best substrate for Ddn in the present study, with a k_{cat}/K_m of 4470 M^{-1} s^{-1}, but was not the most potent at inhibiting *M. tuberculosis* growth (MIC 0.25 μg/ml).

Table 3. Characterization of nitroimidazopyrazinones with extended side chains.

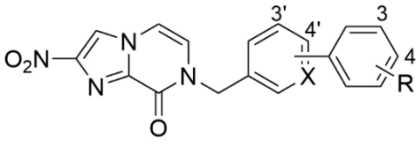

A2

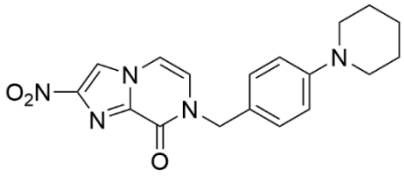

A3

Compd	Form	X	link	R	k_{cat} (s^{-1})	K_M (μM)	k_{cat}/K_M (M^{-1} s^{-1})	Antibacterial MIC (μg/mL)	
								H37Rv normoxia	H37Rv hypoxia
65	A2	C	4'	3-OCF_3	$3.1\times10^{-3} \pm 3.1\times10^{-4}$	8.4 ± 2.4	370	2 (1–8)	32
69	A2	N	4'	3-OCF_3	$1.3\times10^{-3} \pm 7.2\times10^{-5}$	5.0 ± 0.9	266	4 (2–16)	>32
70	A2	N	3'	4-OCF_3	$1.2\times10^{-2} \pm 4.1\times10^{-4}$	2.6 ± 0.36	4470	0.25 (0.25–1)	82–88% I at 4–32 μg/mL
72	A2	N	3'	3-OCF_3	$1.4\times10^{-2} \pm 6.3\times10^{-4}$	4.3 ± 0.57	3190	2 (0.125–4)	84% I at 32 μg/mL
75	A3	-	-	-	$1.7\times10^{-3} \pm 7.8\times10^{-5}$	2.2 ± 0.46	773	1–2	8

% I indicates percentage of inhibition. For compounds with varied MIC in different replicates (n = 3–6), a median value was reported with the MIC range indicated in parentheses.

Exploring alternative scaffolds, nitroimidazoimidazolone and nitroimidazopyrimidinone

The electrochemical study of nitroimidazopyrazinone derivatives revealed a relatively limited range of E′, as the influence of monocyclic side chain substituents on the ease of reduction of the nitro group was minimal. Therefore in this study, modification of the pyrazinone component that was conjugated to the nitroimidazole ring was examined, with the expectation it would be more likely to perturb the electronic properties. Noting the importance of the nitro group and imidazole ring in the biological activity for most nitroimidazoles, including **4**,[35, 52] we focused on retaining these components by modifying the 7-

substituted pyrazinone ring of the current nitroimidazopyrazinone template. A recent study reported by Thompson et al. utilized a scaffold hopping approach to synthesize 7-substituted nitroimidazooxazines that resembled the imidazooxazole core of **3** but with a one carbon expansion.[53] In their study the aromatic side chain of imidazooxazine was moved from the 6-position to the 7-position, and the linker was inverted and attached to the 7-position. This new bicyclic subclass was not only active against *M. tuberculosis* but also highly effective in treating leishmaniasis and Chagas disease.[53] Therefore, a similar strategy of relocating the aromatic side chains to different positions in the new template was employed, resulting in the formation two new scaffolds, nitroimidazoimidazolone **92** and nitroimidazopyrimidinone **93** (Figure 3).

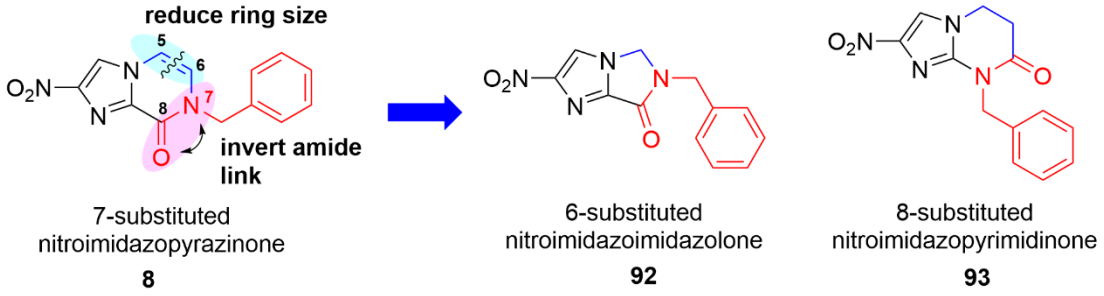

Figure 3. New bicyclic nitroimidazole scaffolds, nitroimidazoimidazolone and nitroimidazopyrimidinone that mimic the existing template, nitroimidazopyrazinone.

The synthesis of the new 6-substituted nitroimidazoimidazolone analog **92** was initiated by preparing the 4(5)-nitroimidazole carboxamide **96**, followed by cyclisation using chloroiodomethane to form the desired imidazolone ring (Scheme 1). This scaffold has a reduced ring size compared to nitroimidazopyrazinones, simulating the 5-membered ring of **3** that can be substituted at the 6-position (Figure 4a). Briefly, nitrated imidazole carboxylic acid **94** was first synthesized,[34] then subjected to reaction with oxalyl chloride and catalytic DMF to yield an acid chloride intermediate **95**. The crude **95** was immediately added to benzylamine in the presence of triethylamine at 0 °C to produce **96**. Triethylamine was added in this case to prevent the conversion of amine to the unreactive HCl salt.[54] In

the final step, intramolecular cyclisation between the imidazole ring amine substituent and the primary/secondary amide linker was accomplished by using 1.5 equivalent of K_2CO_3 under microwave irradiation at 100 °C.

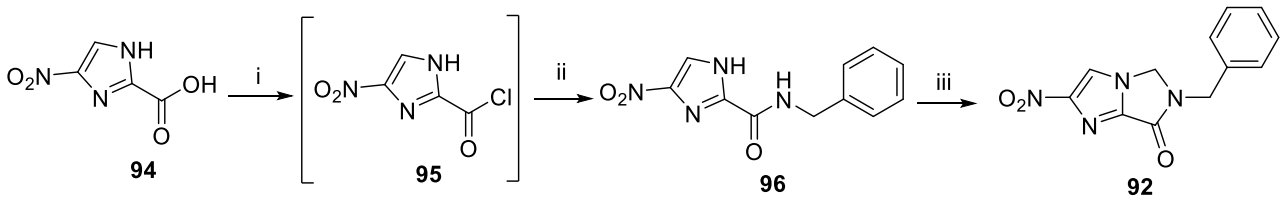

Scheme 1. Synthesis of 6-substituted nitroimidazoimidazolone **92**: (i) oxalyl chloride, catalytic DMF, DCM, 0 °C to room temperature; (ii) benzylamine, TEA, DCM, 0 °C to room temperature, 70% (2 steps); (iii) chloroiodomethane, K_2CO_3, DMF, μW 100 °C, 27%.

To explore alternative side chain positions, a new nitroimidazopyrimidinone scaffold was synthesized by inverting the amide bond of pyrazinone core. This new 8-substituted imidazopyrimidinone **93** could potentially display a different biological profile than the 7-substituted imidazopyrazinone, as the side chain will project at different orientations in the binding pocket of target/activating enzymes (Figure 4b). The synthesis of **93** was performed according to Scheme 2. Chloropropionic acid **97** was first treated with oxalyl chloride to yield the acid chloride intermediate **98**, followed by acylation with benzylamine to form chloropropionamide **99**. Alkylation of **99** with bromo-nitroimidazole at 150 °C using K_2CO_3 under microwave condition resulted in poor yield, mostly due to a secondary reaction – self-cyclisation of **99** to produce 1-benzylazetidin-2-one. However, this reaction serendipitously formed the desired imidazopyrimidinone **93** in a one-pot reaction, albeit at a sub-optimum yield. Increasing the reaction temperature improved the conversion into alkylated product **100** but reduced the yield of **93** in one-pot reaction.

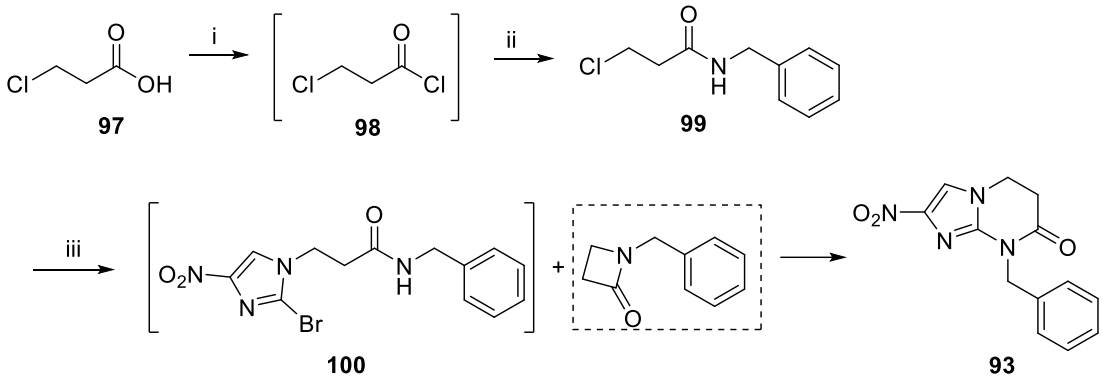

Scheme 2. Synthesis of 8-substituted nitroimidazopyrimidinone **93**: (i) oxalyl chloride, catalytic DMF, DCM, 0 °C to room temperature (ii) benzylamine, TEA, DCM, 0 °C to room temperature, 64% (2 steps); (iii) 2-bromo-4-nitro-1*H*-imidazole, K_2CO_3, DMF, μW 150 °C, 12%.

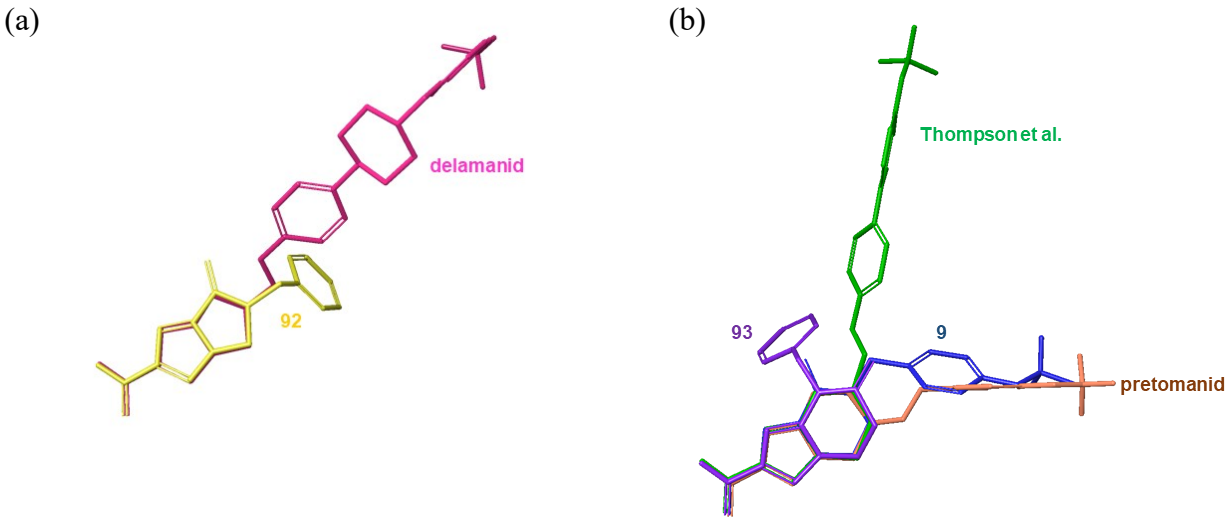

Figure 4. (a) Overlay of 3-dimensional structures of delamanid **3** and nitroimidazoimidazolone **92**. (b) Structure comparison of pretomanid **4**, nitroimidazopyrazinone **9**, nitroimidazopyrimidinone **93** and a new oxazine structure developed by Thompson et al.

Antimycobacterial activity and electrochemical properties of nitroimidazo-imidazolone/-pyrimidinone

The activity of nitroimidazoimidazolone **92** and nitroimidazopyrimidinone **93** was determined against *M. tuberculosis* H37Rv under aerobic and hypoxic growth conditions. Lipophilicities were estimated using Pipeline Pilot (Accelrys, Version 9.1.0.13). Solubility was measured in water and phosphate buffered saline (PBS), pH 7.4 using LC-UV. To determine whether redox activation correlated with antimycobacterial activity of these new scaffolds, formal potential was also examined in anhydrous DMSO. It was found that both nitroimidazo-imidazolone/-pyrimidinone derivatives completely lost antitubercular activity despite having improved solubility (Table 4) compared to the nitroimidazopyazinone **8**. This suggests the importance of the pyrazinone component as a pharmacophore to retain bioactivity against *M. tuberculosis*. The result is also consistent with the inactivity of pyrazine **87** as shown in Table 1. Nitroimidazopyrimidinone **93** had significantly improved solubility (>40-fold) compared to the corresponding pyrazinone **8**, even though it showed higher lipophilicity than **8**. Given that chemical modifications on the pyrazinone component will affect the electronic properties of the nitroimidazole ring and therefore affect the reduction potential, the structure-electrochemical properties relationship was explored (Figure 5). Compound **93** with a saturated 6-membered ring had ~150 mV more negative E′ value than the unsaturated pyrazinone **8**. As a result of the saturation, **93** was not favored at stabilizing the one electron reduced form. It was also kinetically unstable as it underwent a rapid chemical reaction after reduction, similar to **4**. Nitroimidazoimidazolone **92** displayed an equivalent E′ to metronidazole and was easier to reduce than **93**. However, similar to the trend of nitroimidazopyrazinones, the ease of reduction of new scaffolds was not correlated to their bioactivity against *M. tuberculosis*.

Table 4. Physicochemical properties, antimycobacterial activity and reduction potential of new scaffolds.

Compound	AlogP	Solubility (μM)		Antibacterial MIC (μg/mL)		E′ (mV) vs Fc
		water	PBS	H37Rv normoxia	H37Rv hypoxia	
8	0.982	3.2	2.7	0.5–1	4–8	ND
92	1.56	5.9	5.9	>32	>32	-1586
93	1.74	137	142	>32	>32	-1708

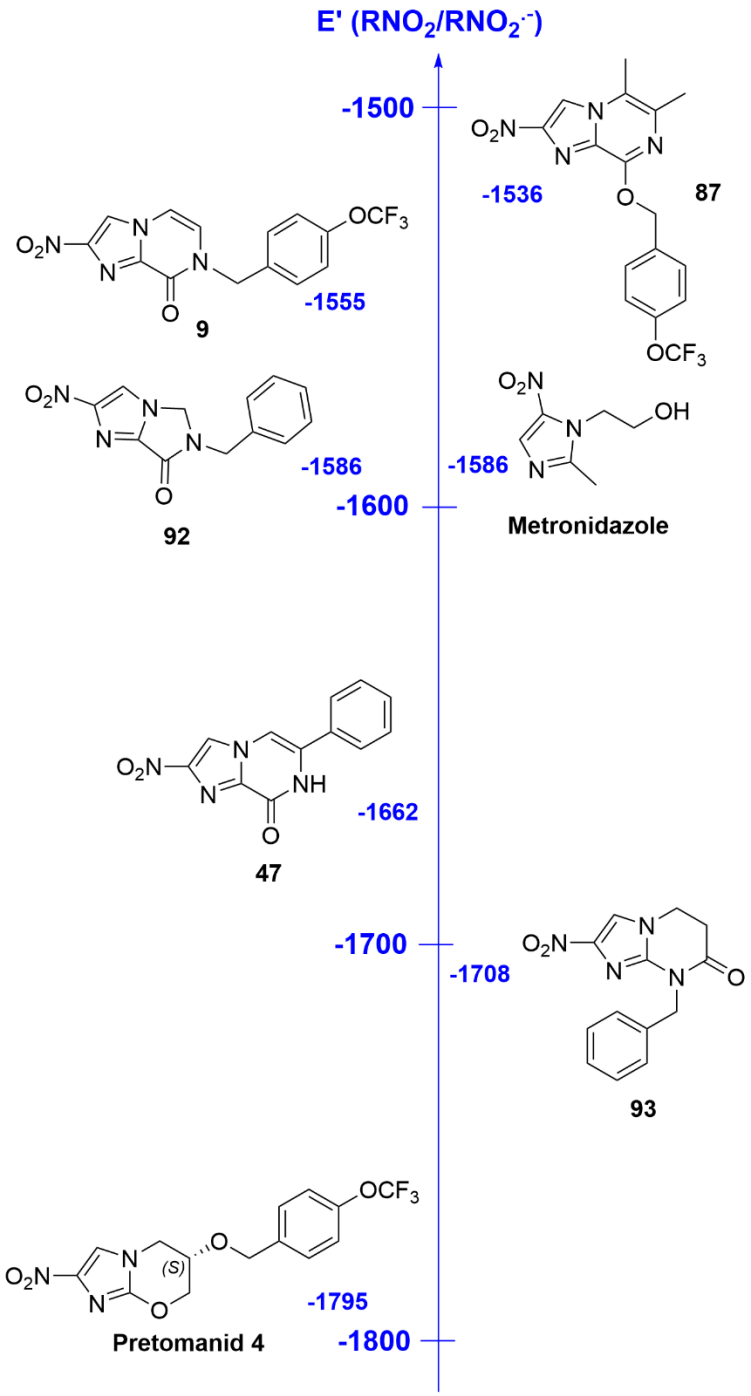

Figure 5. Relationship between electrochemical properties and structural variations of different nitroimidazoles.

Pharmacokinetic profile of compounds 9, 12, 14 and 47

To further assess the potential for potent nitroimidazopyrazinones to be pursued as lead compounds for preclinical development, mouse *in vivo* pharmacokinetic (PK) studies were performed on analogs **9**, **12**, **14** and **47**. These compounds have been previously evaluated for their drug-like properties[34] including microsomal stability, plasma stability, and plasma protein binding (Table 5). To ensure compound solubility prior to the PK study, **9**, **12** and **14** were formulated at 5 mg/mL in 10% DMSO and 90% PEG400, while **47** which possessed higher aqueous solubility, was prepared in a solution of 10% DMSO/40% PEG400/20% cremophor in water. The solutions were then administered to male CD-1 mice both orally and intravenously at 20 mg/kg and 5 mg/kg, respectively. Plasma samples were collected at different time points and analyzed by LC-MS/MS. The mean plasma concentration–time profiles are shown in Figure 6 and the key *in vivo* PK properties are summarized in Table 6. All compounds tested showed moderate to excellent oral bioavailability (F), with F = 64–98%. At a comparable dose, the more soluble **47** reached the highest peak plasma concentration (C_{max}) at 13 µg/mL and exposure ($AUC_{0\text{-}last}$) at 88.3 µg.h/mL. Compound **47** also displayed similar absorption as pretomanid **4** at T_{max} of 2 h (data obtained from literature[55]). When administered intravenously, the volume of distribution (V_{ss}) of **47** was 2.2-fold less than the total body water content (0.73 L/kg), indicating that it was more confined within the plasma, thus less distributed in tissues. Potent antitubercular analogs (**9**, **12** and **14**) showed moderate to high absorption with a T_{max} of 2.7–5.3 h. Their oral C_{max} was in the range of 2.9–3.4 µg/mL and exposure was within 15.6–38.9 µg.h/mL. Although the systemic plasma exposure of **9** and **14** was lower (probably due to their high plasma protein binding), their plasma concentrations remained above MIC values for at least 8 h (Figure 6). Therefore, they have the potential to be administered once daily.

Table 5. *In vitro* ADME properties of pretomanid **4**, compounds **9**, **12**, **14** and **47**.

Compound	**Solubility (µM)**	**PPB (%)**	**Microsomal stability (% remaining at 2 h)**	**Plasma stability (% remaining at 2 h)**

		Human	Mouse	Human	Mouse	Human	Mouse
Pretomanid 4	12	97	91	97	92	96	96
9	<1	>99	>99	>99	>99	98	>99
12	5.4	>99	>99	>99	97	99	97
14	2.9	96	92	ND	ND	ND	ND
47	27	ND	ND	ND	ND	ND	ND

Values are presented as mean of three replicates. Some of the data were reported previously.[34] Solubility in water was determined by LC-UV (254 nm). Microsomal stability control, verapamil at 30 min = 9% (human), 2% (mouse). Plasma stability control, eucatropine at 2 h = 28% (human), 29% (mouse). % bound of PPB control, sulfamethoxazole = 57% (human), 9% (mouse). ND - not determined.

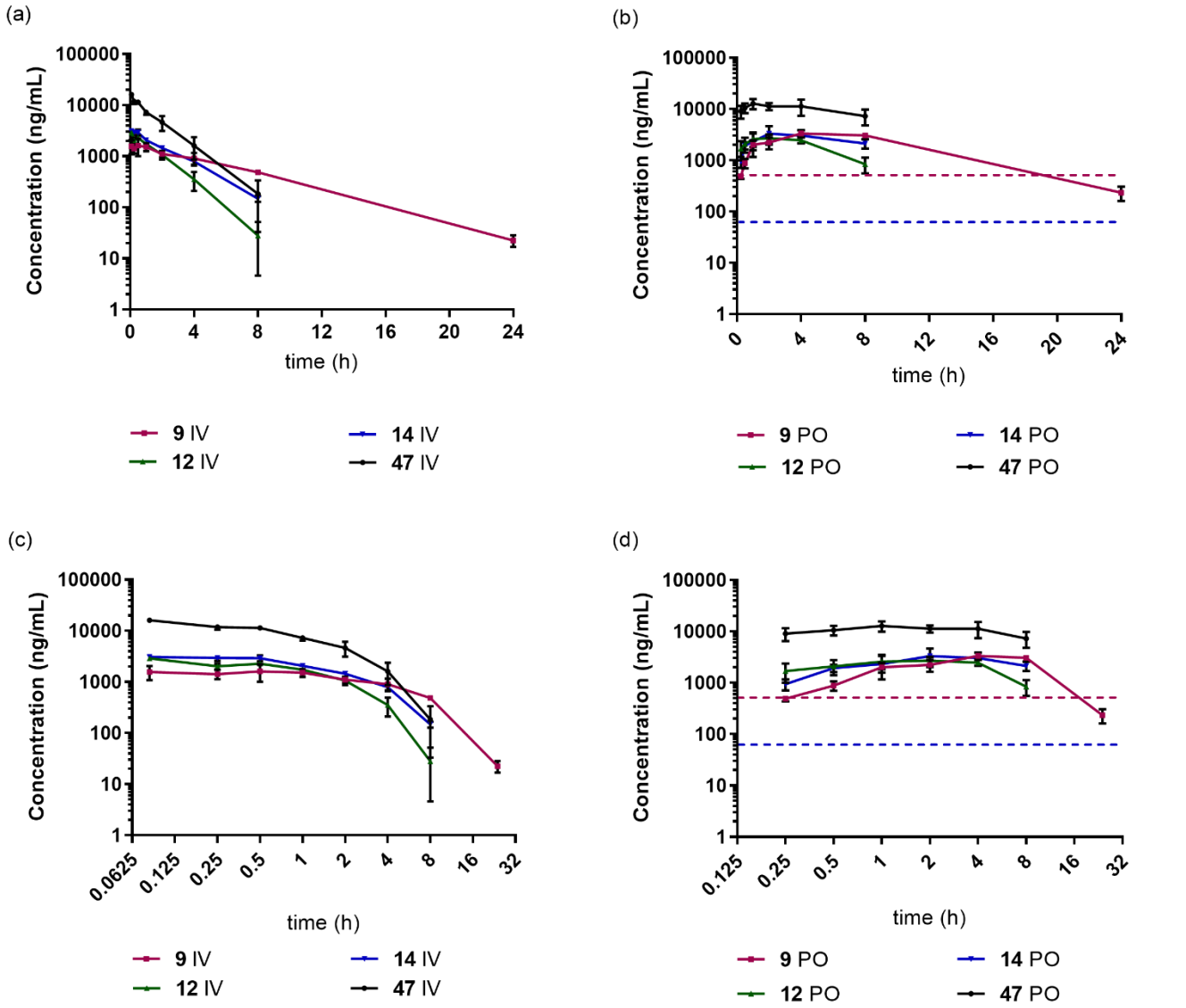

Figure 6. Plasma PK profiles of **9**, **12**, **14** and **47** after intravenous (IV, 5 mg/kg) and oral (PO, 20 mg/kg) administration in linear (a, b) and log (c, d) time scale. Data are shown as mean ± SD from three mice at different time points. Concentrations at 24 h were not determined for **12**, **14** and **47** as they were below the limit of quantitation. The *in vitro* MIC of **9** and **14** against *M. tuberculosis* H37Rv are shown as purple and blue dashed lines, respectively.

Table 6. *In vivo* pharmacokinetic properties of selected analogs.

Route	PK parameters	Pretomanid 4*	9	12	14	47
PO	Formulation	2.5 mg/mL in 10% hydroxypropyl-β-cyclodextrin/ 10% lecithin/ 80% water	5 mg/mL in 10% DMSO/90% PEG400	5 mg/mL in 10% DMSO/90% PEG400	5 mg/mL in 10% DMSO/90% PEG400	2 mg/mL in 10% DMSO/40% PEG400/20% cremophor RH40/30% water
	Dose (mg/kg)	25	20	20	20	20
	C_{max} (µg/mL)	6.0	3.3	2.9	3.4	13
	$AUC_{0\text{-last}}$ (µg.h/mL)	50.9	38.9	15.6	20.8	88.3
	T_{max} (h)	2	5.3	3	2.7	2
	$T_{1/2}$ (h)	2.7	4.8	ND	ND	3.2
	F (%)	100	98	73	64	87
IV	Formulation	2 mg/mL in 10% hydroxypropyl-β-cyclodextrin/ 10% lecithin/ 80% water	5 mg/mL in 10% DMSO/90% PEG400	5 mg/mL in 10% DMSO/90% PEG400	5 mg/mL in 10% DMSO/90% PEG400	2 mg/mL in 10% DMSO/40% PEG400/20% cremophor RH40/30% water
	Dose (mg/kg)	10	5	5	5	5
	V_{ss} (L/kg)	1.6	2.2	1.1	1.2	0.34
	CL (mL/min/kg)	12.1	6.36	10.1	7.66	3.38
	$T_{1/2}$ (h)	1.6	3.8	1.1	1.9	1.2

C_{max} = maximum concentration reached in plasma, $AUC_{0\text{-last}}$ = exposure between 0 to last time point (8h for **12**, **14** and **47**; 24 h for **9**), T_{max} = time to reach maximum concentration, $T_{1/2}$ = half-life, F = oral bioavailability, V_{ss} = volume of distribution at steady state, CL = total systemic clearance, ND = not determined (due to inadequately defined terminal elimination phase). *Results obtained from literature [55].

Efficacy in TB mouse models

Two analogs, **9** and **14**, were selected for assessment of efficacy in an acute BALB/c mouse *M. tuberculosis* infection model. These compounds were chosen based on their promising *in vitro* activity against both replicating and non-replicating *M. tuberculosis*, good PK profile as well as high k_{cat}/K_M values with Ddn. *M. tuberculosis* was inoculated into the lung by aerosol at Day 0, and treatment started at Day 10, with pretomanid **4** and rifampicin used as positive controls. Following three weeks of oral treatment, the levels of colony-forming units (CFU) in lungs were measured, with the test compounds at three different concentrations producing a dose-dependent response (Figure 7). The lung bacterial burden of the untreated group increased from 8.8 x 10^3 CFU to 1.1 x 10^6 CFU. Compound **14** was more efficacious than **9** ($P < 0.001$), reducing the bacterial load by 0.75, 1.1 and 1.7 log CFU at 12.5, 25 and 50 mg/kg, respectively. At the highest dosing (50 mg/kg), **14** showed comparable activity to **4** dosed at 20 mg/kg. Compound **9** was moderately active, with efficacy ranging from 0.21–0.72 log reduction in CFU compared to the vehicle control. Rifampicin was used as an additional control (Supporting information, Figure S4) and gave 2.7 log CFU reduction of bacterial load at 15 mg/kg. No mortality or obvious weight loss was found during the course of treatment, indicating the compounds were well-tolerated at the doses evaluated (Supporting information, Table S1).

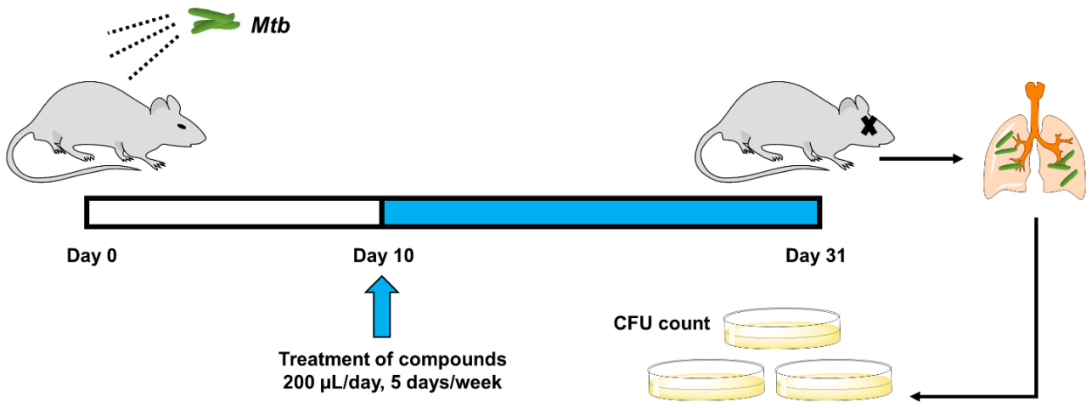

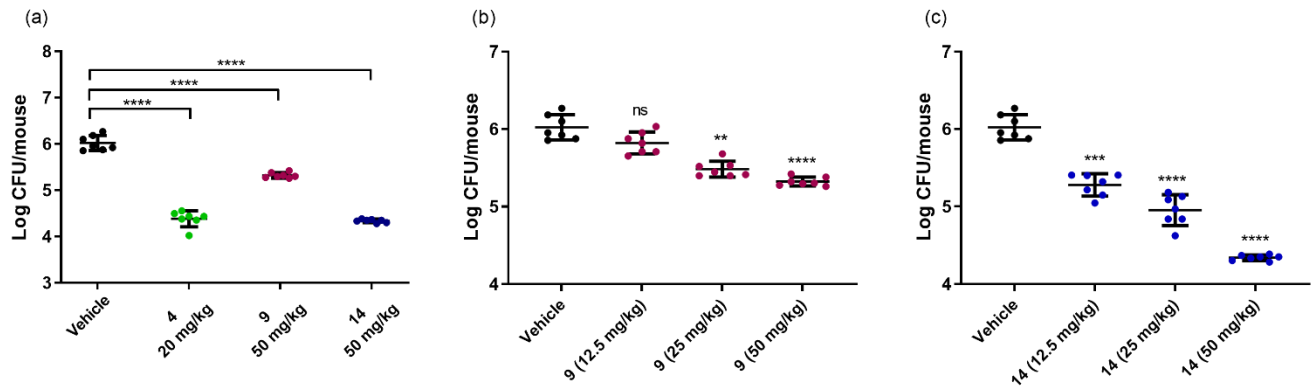

Figure 7. Treatment schedule in BALB/c mouse models of acute *M. tuberculosis* infection. *M. tuberculosis* was inoculated into the lung by aerosol at Day 0, and treatment started at Day 10. At day 31, mice were sacrificed and lungs were removed, homogenized, and plated onto 7H11 agar to determine the bacterial load. (a) CFU count data in the lungs of infected mice treated with vehicle, pretomanid **4**, compounds **9** and **14**; dose response of (b) **9** and (c) **14** at 12.5, 25 and 50 mg/kg. Statistical significance was determined by ordinary one-way ANOVA followed by Dunnett's multiple comparison test. ****$P < 0.0001$, ***$P < 0.001$, **$P < 0.01$, ns - not significant.

Antitrypanosomal activity of extended side chains of nitroimidazopyrazinones

The repurposing potential of **3** and **4** analogs for the treatment of kinetoplastid diseases[19, 21, 22] led us to investigate the antitrypansomal activity of nitroimidazopyrazinones against *T. cruzi*. Initial investigations using high content imaging demonstrated that analogs with extended biaryl side chains were highly active against *T. cruzi* (IC_{50} = 0.016–4.2 μM).[37] This assay utilized an incubation time of 48 h, as longer incubation periods could bias the assay to identify *T. cruzi* cytochrome P450 (TcCYP51) inhibitors that are slow acting.[56]. Early prediction of potential CYP inhibitors that are sub-efficacious is also possible with a 48 hour incubation.[57] As CYP51 is a promiscuous target in Chagas disease, targeting it has resulted in the failures of many clinical candidates including azole compounds (such as posaconazole). Therefore compounds that are fast-acting and long-lasting are often prioritized in drug discovery campaigns.[58] Of

a total of 16 biaryl analogs, **73** and **74** were selected for further *in vivo* efficacy. Compound **73** was the most potent analog across the series when tested *in vitro* (IC_{50} of 0.016 μM, selectivity index of >2220), while **74** (IC_{50} of 0.10 μM, selectivity index of >353) was favored due to its better solubility, especially in acidic conditions (>200 μM). These compounds completely cleared parasites (100%) from 3T3 host cells at E_{max} concentrations (maximal activity achievable in dose-response curves, Figure 8), in contrast to the CYP51 inhibitor, posaconazole that showed 87% inhibition at E_{max}. This phenotypic characteristic suggested that **73** and **74** might not inhibit the CYP enzyme, consistent with other bicyclic nitroimidazole analogs that were reported to be inactive against CYP51.[22]

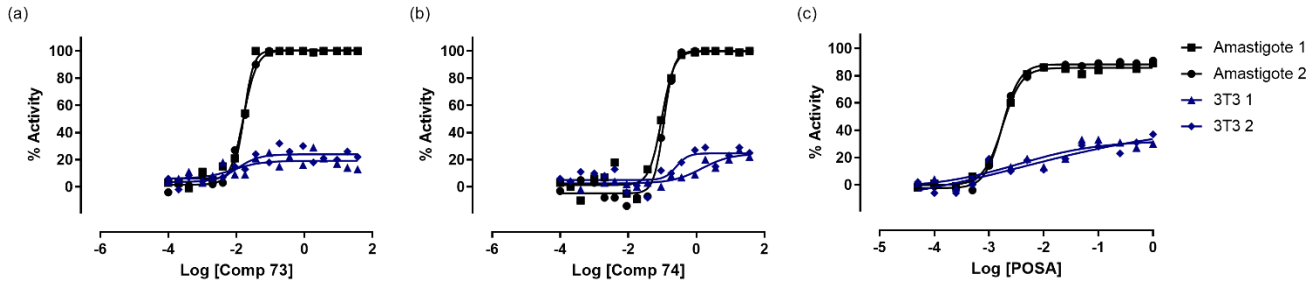

Figure 8. Dose-response curves for (a) **73**, (b) **74**, and (c) posaconazole (POSA) against *T. cruzi* amastigotes in 3T3 cells and their activity against 3T3 cells. The IC_{50} values of **73** and **74** were 0.016 ± 0.0003 μM and 0.10 ± 0.005 μM, with E_{max} of 100%.

Pharmacokinetic profile of 73 and 74

The antiparasitic agents, **73** and **74** had distinctly different pharmacokinetic profiles (Figure 9, Table 7). Compound **74** had the fastest absorption rate (T_{max} = 0.67 h) among the nitroimidazopyrazinones investigated, while absorption of **73** was ~10-fold slower, presumably due to its higher lipophilicity. Consistent with the mouse microsomal stability study (Table 8),[37] **74** exhibited a short half-life (<1 h) when dosed orally. Despite having lower exposure due to its high clearance and high V_{ss}, **74** demonstrated good oral bioavailability at 92%. In contrast, **73** had the longest half-life (6.1 h oral, 7.2 h

IV) compared to other analogs including the monocyclic side chains **9**, **12** and **14**. Plasma concentrations of **73** reached a C_{max} at 5.3 h and remained above its *in vitro* IC_{50} for more than 24 h (Figure 9). However **73** showed lower bioavailability (F = 45%), which is likely associated with its slower absorption and poor solubility.

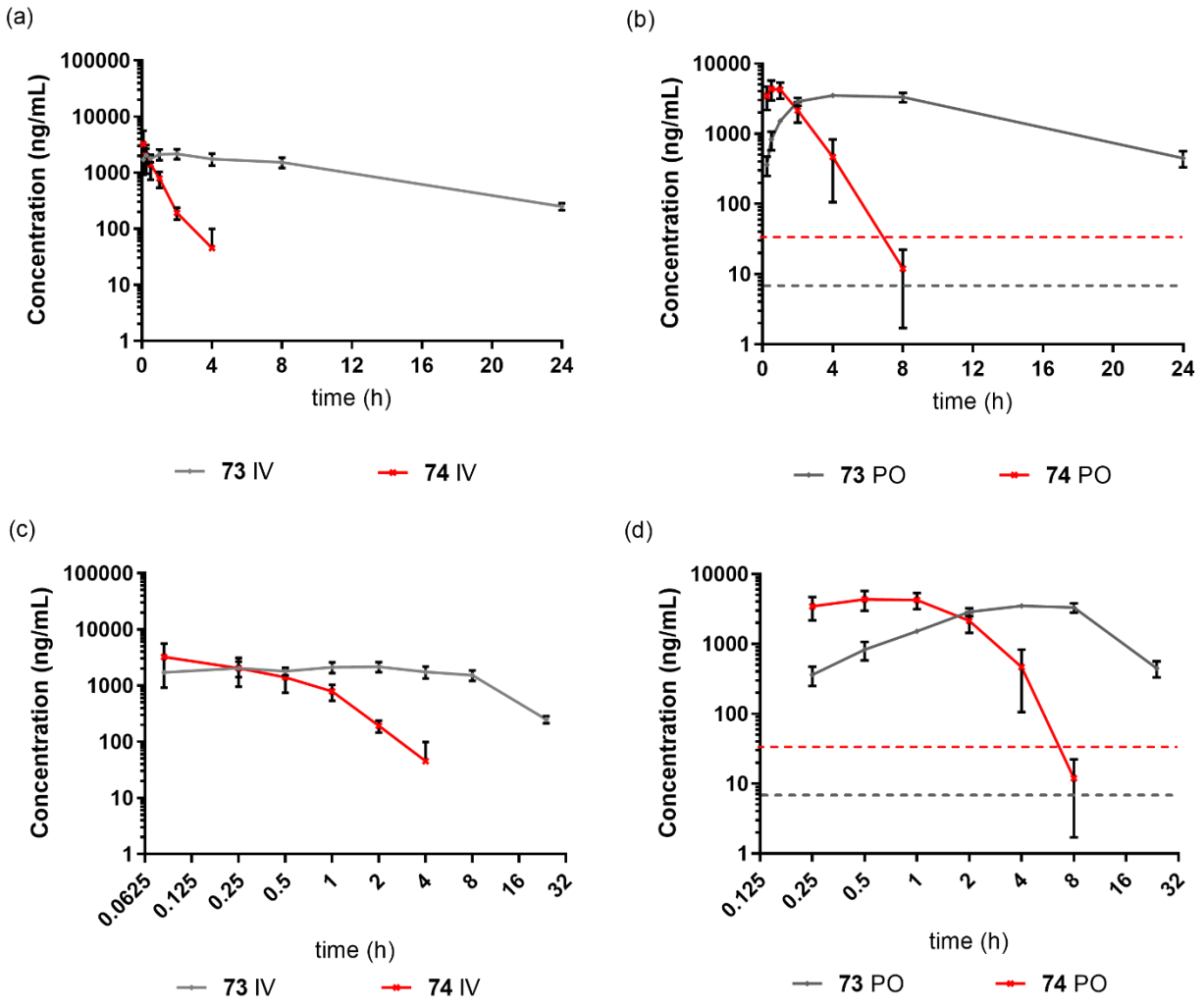

Figure 9. Plasma PK profiles of **73** and **74** after intravenous (IV, 5 mg/kg) and oral (PO, 20 mg/kg) administration in linear (a, b) and log (c, d) time scale. Data are shown as mean ± SD from three mice at different time points. Concentration at 24 h was not determined for **74** as it is below the limit of quantitation. The *in vitro* IC_{50} of **73** and **74** against *T. cruzi* are shown as grey and red dashed lines.

Table 7. *In vivo* pharmacokinetic properties of anti-*T. cruzi* agents, **73** and **74**.

Route	PK parameters	73	74
PO	Formulation	5 mg/mL in 10% DMSO/90% PEG400	5 mg/mL in 10% DMSO/90% PEG400
	Dose (mg/kg)	20	20
	C_{max} (µg/mL)	3.6	4.5
	$AUC_{0\text{-}last}$ (µg.h/mL)	45.9	9.26
	T_{max} (h)	5.3	0.67
	$T_{1/2}$ (h)	6.1	0.77
	F (%)	45	92
IV	Formulation	5 mg/mL in 10% DMSO/90% PEG400	5 mg/mL in 10% DMSO/90% PEG400
	Dose (mg/kg)	5	5
	V_{ss} (L/kg)	1.3	2.6
	CL (mL/min/kg)	2.06	22.9
	$T_{1/2}$ (h)	7.2	1.5

In vivo efficacy study in a bioluminescent *T. cruzi* mouse model

As a proof of concept, compounds **73** and **74** were evaluated for their *in vivo* activity using an acute *T. cruzi* infected murine model and bioluminescence imaging. BALB/c mice (n=3/group) infected with bioluminescent *T. cruzi* CL Brener parasites (see Materials and Methods) were treated at the peak of the acute stage infection (14 dpi). The untreated group (vehicle only) displayed high parasitemia levels until 24 dpi, whereas mice treated with **73** and **74** showed a reduction in parasite burden of >98–99% by 18 dpi that persisted until 24 dpi (Figure 10). A similar outcome was observed in mice treated with benznidazole **1** at 100 mg/kg. However, all mice were bioluminescence positive by 36 dpi. Both **73** and **74** were able to transiently reduce the parasite burden to background levels by the end of treatment, with no significant adverse effects observed in all mice treated with both compounds (a slight weight loss was noticed in mice treated with **1**). Although not significant, at 36 dpi the bioluminescence intensity was more intense in the mice treated with **1** compared to the mice that were treated with both **73** and **74** (Figure 10).

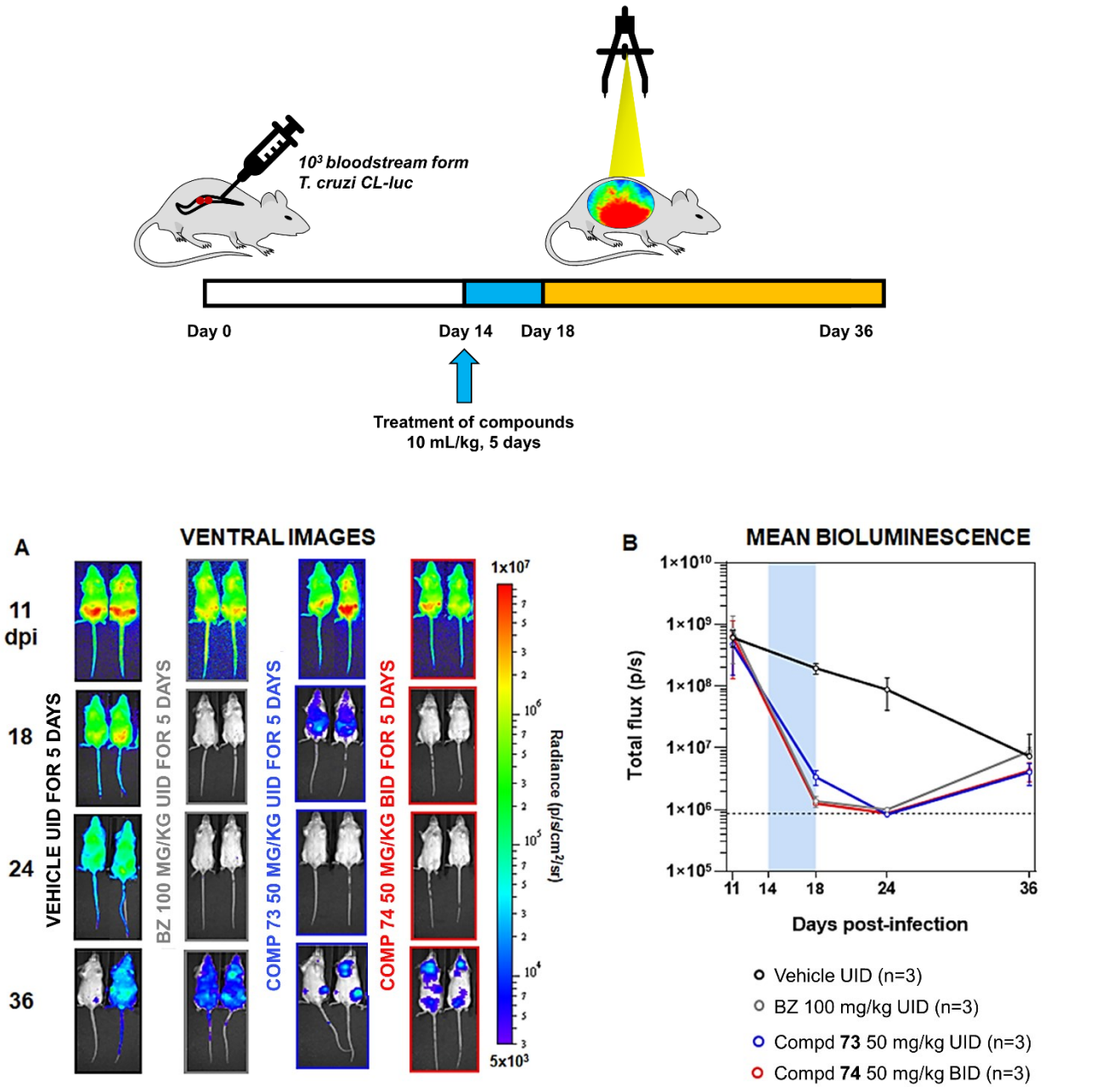

Figure 10. *In vivo* assessment of compounds **73** and **74** as a treatment for experimental acute stage *T. cruzi* infections. (A) Representative ventral images of two BALB/c mice infected with bioluminescent CL-Brener were treated at the acute stage of infection (day 14) with vehicle (orally, 5 days, once daily, n=3), benznidazole **1** (BZ) at 100 mg/kg (orally, 5 days, once daily, n=3), **73** at 50 mg/kg (orally, 5 days, once daily, n=3) and **74** at 50 mg/kg (orally, 5 days, twice daily, n=3) and followed until 36 days post-

infection (dpi). Heat-maps are on $\log^{10}$ scales and indicate intensity of bioluminescence from low (blue) to high (red). At day 36 post-infection, all mice were humanely killed. (B) Mean bioluminescence evaluation of mice treated with **73** and **74** during acute stage *T. cruzi* infections. Treatment groups, dose regimens, including time of treatment (blue bar), are indicated.

Table 8. Activity profile of nitroimidazopyrazinones with biaryl side chains.

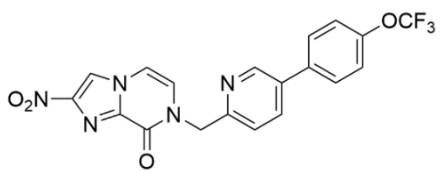

73

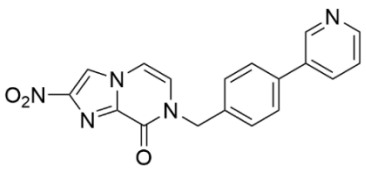

74

Compd	Solubility[a] (µM)		*T. cruzi* amastigotes			3T3 CC_{50} (µM)	Selectivity index	PPB (%)[d]		Microsomal stability[d] (% remaining at 2 h)		Plasma stability[d] (% remaining at 2 h)		*In vivo* efficacy (% reduction in parasite burden)
	water, pH 7	0.1 M HCl, pH 1	IC_{50} (µM)	IC_{90} (µM)	% activity at Emax			Human	Mouse	Human	Mouse	Human	Mouse	
Benznidazole 1	ND	ND	7.6	28	100	>127	>17	ND	ND	ND	ND	ND	ND	99.3
Posaconazole	ND	ND	0.0020	0.0040	87	>1	>569	ND	ND	ND	ND	ND	ND	ND
9	<1	<1	0.15	0.72	100	>73	>507	98	ND	>99	>88	98	>99	ND
73	<1	3.7	0.016[b]	0.039	100	>37	>2220	>99	>99	>99	98	>99	>99	98.3
74	3.9	>200	0.10[c]	0.24	100	>37	>353	96	93	96	20	93	>99	99.4

[a] Solubility in water and HCl was determined by LC-UV (254 nm); [b] equivalent to 0.0069 µg/mL; [c] equivalent to 0.035 µg/mL; [d] data reported previously [37]. Values are presented as mean of three replicates. Microsomal stability control, verapamil at 30 min = 9% (human), 2% (mouse). Plasma stability control, eucatropine at 2 h = 28% (human), 29% (mouse). % bound of PPB control, sulfamethoxazole = 57% (human), 9% (mouse). ND - not determined

Conclusion

Nitroimidazoles were once considered to be 'undesirable' in drug discovery due to the possible toxicity issues associated with the nitro group. However, recent advances have demonstrated that new nitroaromatics with favorable therapeutic indices are possible by controlling the bioactivation of the nitro groups. This study has expanded our prior work to further explore the properties of nitroimidazopyrazinones as a new bicyclic subclass capable of treating both tuberculosis and CD. Nitroimidazopyrazinones were found to be highly selective at killing *M. tuberculosis*, but were not active against nontuberculosis mycobacteria. Chemical modifications of the pyrazinone ring led to novel nitroimidazo-imidazolone/-pyrimidinones but these modifications were detrimental to the antitubercular activity. Through enzymatic screening against deazaflavin-dependent nitroreductase (Ddn), a subset of nitroimidazopyrazinones were identified as effective substrates. Although there was some good correlation between enzymatic activity and mycobacteria killing, it should be noted that the kinetic parameters of Ddn is only a reflective of $F_{420}H_2$ reoxidation and does not translate directly into the whole cell activity. A more detailed biochemical analysis such as measuring the kinetics of NO production by Ddn may provide greater insight into their mode of action in *M. tuberculosis*. In the future, a comparison of activity against Ddn mutants or other homologues such as Rv1261c, Rv1558 and Rv3178 could assess the specificity of this Ddn-mediated bioactivation. As resistance towards nitroimidazoles have been found to already be present due to mutations in Ddn, assessing and developing new compounds that can be activated by more than one F_{420}-dependent enzyme would be of great benefit.[41, 59]

Electrochemical properties were determined by cyclic voltammetry but there was not a clear correlation between ease of reduction of nitroimidazoles and their bioactivity. It is possible that nitroimidazopyrazinones exert their activity through several pathways, and therefore a single parameter

(such as Ddn catalytic efficiency and redox potential) will not correlate perfectly to their potency. These multiple targeting mechanisms can potentially be used to overcome or delay the rise of resistance.

Compound **14** was identified as the most promising hit compound against *M. tuberculosis*, with satisfactory pharmacokinetic profile and high efficacy in acute TB mouse models. A different subset of nitroimidazopyrazinones, with extended biaryl side chains, demonstrated sub-micromolar inhibitory activity against *T. cruzi in vitro* and were able to suppress infection *in vivo* in a mouse model. Compound **74** with a terminal pyridine side chain (pyridine-3-yl-phenyl group), demonstrated improved solubility and oral bioavailability (F=92%) compared to **73** (4-trifluromethoxyphenyl-3-pyridine group), while **73** displayed a longer half-life and could be used for once daily dosing. Due to the absence of Ddn in *T. cruzi*, it was postulated that other nitroreductases such as NTR2 homolog or old yellow enzyme,[31] might involve in the bioactivation of these bicyclic nitroimidazoles. Given that nitroimidazoles are known to exert their bioactivity through production of various reactive species, this could obscure the concentration-response relationship. Hence, a standard pharmacokinetic/pharmacodynamic correlation is not necessarily implied in our case.

Taken together, our work has revealed the potential of a new bicyclic nitroimidazole subclass for the treatment of tuberculosis and Chagas disease, supported by *in vivo* pharmacokinetic and efficacy studies that demonstrate the potential for active nitroimidazopyrazinones to be developed as clinical candidates. Further exploration of their multiple mode of actions under both aerobic and hypoxic conditions could help understand their capacity to target drug-resistant organisms, while additional *in vivo* studies could optimise dosing regimens and evaluate efficacy against both chronic and acute infections.

General Experimental

All the reagents and solvents were obtained from commercial sources and were used without further purification. Progression of reaction was monitored by TLC using Merck alumina sheets pre-coated with silica gel 60 F254 and was visualised using a UV lamp. Purification of compounds was done using a Biotage Isolera or Grace Reveleris chromatography system. NMR data were collected at 298K on a Varian Unity 400 MHz or Bruker Advance 600 MHz spectrometer. Chemical shifts were measured relative to tetramethylsilane or the residual solvent signals (DMSO-d_6) as the internal reference. Data are presented as follows: chemical shift (ppm), multiplicity (s = singlet, d = doublet, t = triplet, q = quartet, m = multiplet, bs = broad singlet) and coupling constant (Hz). Analytical LC-MS was performed on a Shimadzu LCMS-2020 using 0.05% formic acid in water (solvent A) and 0.05% formic acid in acetonitrile (solvent B) as mobile phase. LC-MS condition: column Zorbax Eclipse XDB-Phenyl, 3.0×100 mm, 3.5 μm; column temperature: 40 °C; flow: 1 mL/min; gradient timetable: 0.00 min, 5% B; 0.50 min, 5% B; 3.00 min, 100% B; 4.2 min, 100% B; 5.00 min, 5 % BAll final products were >95% pure as determined by LC-MS using UV at 254 nm, ELSD and APCI/ESI-MS. The purity percentage was indicated by Abs %.

Synthesis of nitroimidazopyrazin-ones/-es, 7–90

Nitroimidazopyrazin-one/-e analogs were synthesized according to our recently reported methods.[34, 37] All compounds are >95% pure as determined by liquid chromatography-mass spectrometry (LC-MS) using UV at 254 nm, ELSD and APCI/ESI-MS detectors. Synthetic routes and experimental details are briefly described in Supporting Information Scheme S1. HPLC traces of key compounds (**9**, **14**, **73** and **74**) are included in Supporting Information Figure S5.

Synthesis of nitroimidazoimidazolone

N-Benzyl-4-nitro-1*H*-imidazole-2-carboxamide (96)

4-Nitro-1*H*-imidazole-2-carboxylic acid **94** (180 mg, 1.15 mmol, 1 equiv) was dissolved in 4 mL of anhydrous DCM and chilled at 0 °C under N_2. Oxalyl chloride (194 µL, 2.29 mmol, 2 equiv) was added dropwise over 10 min, followed by addition of DMF (2 drops). The reaction was allowed to warm to room temperature and stirred overnight. Volatiles were removed *in vacuo* and the excess oxalyl chloride was removed by co-evaporation with toluene for two times. The resulting acid chloride crude solid **95** (200 mg, 1.14 mmol, 1 equiv) was then added immediately to 3 mL of anhydrous DCM (15 vol) and triethylamine (318 µL, 2.28 mmol, 2 equiv) on an ice bath. The blue-purple solution was then added dropwise to benzylamine (149 µL, 1.37 mmol, 1.2 equiv) in 5 vol (1 mL) of anhydrous DCM at 0 °C under N_2. After completion of the reaction, volatiles were removed *in vacuo* before purifying over silica gel by MPLC (Biotage Isolera, 20–100% pet. spirits/EtOAc) to give the final product as white solid (198 mg, 70%). LCMS: Rt = 2.69 min, 99 Abs % @ 254 nm, $[M+H]^+$ = 247.1. ^{1}H NMR (600 MHz, DMSO-d_6) δ 9.44 (t, J = 6.4 Hz, 1H), 8.46 (s, 1H), 7.32 (d, J = 4.4 Hz, 4H), 7.24 (tt, J = 4.6, 3.8 Hz, 1H), 4.43 (d, J = 6.4 Hz, 2H). ^{13}C NMR (150 MHz, DMSO-d_6) δ 157.1, 146.7, 139.6, 139.0, 128.2, 127.4, 126.8, 121.2, 42.3.

6-Benzyl-2-nitro-5,6-dihydro-7*H*-imidazo[1,5-*a*]imidazol-7-one (92)

To a stirred solution of *N*-benzyl-4-nitro-1*H*-imidazole-2-carboxamide **96** (40 mg, 0.162 mmol, 1 equiv) in 4 mL (100 vol.) of *N,N*-dimethylformamide was added 2 equiv of potassium carbonate (44.9 mg, 0.325 mmol) and 2 equiv of chloroiodomethane (23.7 µL, 0.325 mmol). The reaction mixture was microwaved at 90 °C for 20 min (separated into two vials), then diluted with distilled water (40 mL) and cooled on an ice bath to cause more precipitation. The precipitate was then filtered, washed with water (2 x 2 mL) and acetonitrile (2 x 2 mL), and dried under vacuum to give 6-benzyl-2-nitro-5,6-dihydro-7*H*-imidazo[1,5-*a*]imidazol-7-one as white solid (10.2 mg, 24%). LCMS: R_t = 2.60 min, 97% Abs @ 254 nm, $[M+H]^+$ = 259.1. ^{1}H NMR (600 MHz, DMSO-d_6) δ 8.62 (s, 1H), 7.41 – 7.27 (m, 5H), 5.47 (s, 2H), 4.75 (s, 2H). ^{13}C NMR (150 MHz, DMSO-d_6) δ 155.4, 150.0, 140.6, 135.8, 128.7, 127.9, 127.7, 119.5,

61.2, 45.2. Dimer peaks were found (4% after integrated). On the other hand, the aqueous filtrate was collected and extracted with EtOAc (3 x 40 mL). The organic layers were collected, washed with brine (40 mL), dried over $MgSO_4$ and the volatiles were removed in *vacuo*. The crude material was purified by HPLC using Water Atlantis C18 prep column (Gilson, 0-100 % H2O +0.05% formic acid, ACN +0.05% formic acid gradient elution) to yield additional cyclised product (white, 1.1 mg, 3%) and dimers (3%).

Synthesis of nitroimidazopyrimidinone

***N*-Benzyl-3-chloropropanamide (99)**

Oxalyl chloride (1.01 mL, 1.20 mmol, 1.3 equiv) was added dropwise to a stirred solution of 3-chloropropionic acid **97** (1 g, 9.21 mmol, 1 equiv) in 20 mL of anhydrous DCM at 0 °C under nitrogen, followed by addition of a catalytic quantity of DMF. The reaction mixture was stirred at rt overnight before concentration under reduced pressure. The crude acyl chloride **98** was dissolved in 23 mL of anhydrous DCM, then added dropwise to a stirring mixture of 0.83 equiv of benzylamine (831 µL, 7.61 mmol) and 1 equiv of trimethylamine (1.27 mL, 9.14 mmol) cooled to 0 °C under nitrogen. After completion of the reaction, volatiles were removed in *vacuo* and further purified by MPLC (Biotage Isolera, 1-10% DCM/MeOH) to give the product as white powder (1.15 g, 64% yield); LCMS: R_t = 2.51 min, 99 Abs % @ 200 nm, $[M+H]^+$ = 228.1; ^{1}H NMR (600 MHz, DMSO-d_6) δ 8.50 (t, J = 6.0 Hz, 1H), 7.35 – 7.29 (m, 2H), 7.27 (s, 1H), 7.29 – 7.20 (m, 2H), 4.30 (d, J = 5.9 Hz, 2H), 3.82 (t, J = 6.3 Hz, 2H), 2.64 (t, J = 6.3 Hz, 2H). ^{13}C NMR (150 MHz, DMSO) δ 168.9, 139.3, 128.2, 127.2, 126.7, 42.1, 41.1, 38.2.

8-Benzyl-2-nitro-5,6-dihydroimidazo[1,2-*a*]pyrimidin-7(8*H*)-one (93)

To a stirred solution of 2-bromo-4-nitro-1*H*-imidazole (50 mg, 0.260 mmol, 1 equiv) in 15 vol (750 µL) of DMF was added 3 equiv of potassium carbonate (108 mg, 0.781 mmol) and 1 equiv of *N*-benzyl-3-

chloropropanamide **99** (61.8 mg, 0.313 mmol, 1.2 equiv). The reaction mixture was microwaved at 150 °C for 20 min, then diluted with 7.5 mL of distilled water and extracted with EtOAC (3 x 7.5 mL). The organic layer was collected, washed with brine (7.5 mL) and dried with $MgSO_4$. Volatiles were removed *in vacuo* and further purified by HPLC (Gilson, A: water, B: ACN, 0–50% B) to give the product as a cream solid (8.5 mg, 12% yield); LCMS: R_t = 2.52 min, 98 Abs % @ 254 nm, $[M+H]^+$ = 273.1; ^{1}H NMR (600 MHz, DMSO-d_6) δ 8.30 (s, 1H), 7.35 – 7.29 (m, 4H), 7.25 (td, J = 6.7, 1.9 Hz, 1H), 5.01 (s, 2H), 4.28 (t, J = 7.1 Hz, 2H), 3.01 (t, J = 7.1 Hz, 2H). ^{13}C NMR (150 MHz, DMSO-d_6) δ 166.2, 144.1, 142.5, 136.5, 128.3, 127.2, 127.2, 120.0, 44.8, 39.8, 30.2. Impurities were detected in ^{1}H NMR analysis at 5% after integration.

Mycobacterial minimum inhibitory concentration assay

The minimum inhibitory concentration (MIC) study was performed against *M. tuberculosis* H37Rv (ATCC 27294), avirulent *M. tuberculosis* H37Ra (ATCC 25177), *M. avium* (ATCC 25291) and *M. smegmatis* mc^{2}155 (ATCC 700084) using a resazurin reduction microplate assay as previously described.[34] Compounds were serially diluted across the 96-well microtiter plates in 100 µL of 7H9S media (7H9 with 10% ADC, 0.5% glycerol, 0.05% Tween-80 and 1% tryptone). *M. tuberculosis* H37Rv, *M. tuberculosis* H37Ra, *M. avium* and *M. smegmatis* were was cultured in Middlebrook 7H9 broth medium supplemented with ADC (Difco Laboratories), 0.5% glycerol, and 0.02% Tyloxapol at 37 °C until mid-exponential phase (OD_{600} 0.4-0.8) before being diluted to the appropriate cell density in 7H9S media and added to the assay plate. Final cell density in the assay plates was ~2×10^4 CFU/mL (OD_{600} 0.001) for *M. tuberculosis* H37Rv, H37Ra & *M. avium* and 4×10^4 CFU/mL (OD_{600} 0.002) for *M. smegmatis*. The plates were then incubated for 5 days for *M. tuberculosis* H37Rv, 6 days for *M. tuberculosis* H37Ra and *M. avium*, and 24 h for *M. smegmatis* at 37 °C in a humidified incubator before the addition of 30 µL of a 0.02% resazurin solution and 12.5 µL of 20% Tween-80 and further incubated

for an additional 24 h at 37 °C. Sample fluorescence was measured on a Fluorostar Omega fluorescent plate reader (BMG) (excitation 530 nm, emission 590 nm).

For hypoxic assays of *M. tuberculosis* H37Rv, the same method was used as the normoxic condition except the plates were incubated for 5 days at 0.1% oxygen before the addition of resazurin and incubated for an additional 48 h prior to fluorescence reading. Percent fluorescence relative to the positive control wells (bacteria without compound) minus the negative control wells (media only) was plotted for the determination of the MIC, the lowest concentration at which the percentage inhibition was ≥90%.

Cyclic voltammetry analysis

The electrochemical study was done using a BAS CV-100 voltammetric analyser. All the voltametric measurements were performed at room temperature in a 5 mL voltametric cell. Oxygen was removed by bubbling argon gas through the sample solution before measurements were taken. Reference electrode used for experiments in anhydrous DMSO and mixed medium (mixture of 70% DMSO and 30% of PBS) was $Ag/AgNO_3$ and Ag/AgCl, respectively. A glassy carbon electrode (BAS) was used as working electrode and a platinum wire served as counter electrode. BAS was polished with 0.05 μm alumina prior to and in the interval of experiments. Supporting electrolytes used were 0.1 M tetrabutylammonium hexafluorophosphate (TBAHFP) for measurements in DMSO and 0.1 M KCl for mixed medium. Compounds were tested at 1 mM concentration. Ferrocene was used as the reference point for the formal potential (E′) measurements in DMSO. Different sweep rates at 50-2000 mVs^{-1} were used.

Protein expression and purification

Deazaflavin-dependent nitroreductase (Ddn) was expressed and purified as previously described.[41] In brief, Ddn enzyme was transformed into *Escherichia coli* BL21 (DE3) and grown on ampicillin-containing Luria-Bertani (LB) agar plates. Single colonies were picked, inoculated in LB media with ampicillin (100 μg/mL) and grown overnight. The overnight cultures were diluted 100x and grown until

OD_{600} 0.4. Expression was induced with isopropyl β-D-1-thiogalactopyranoside (IPTG) to a final concentration of 0.3 mM. Cultures were grown for 3 h at 25 °C before harvested by centrifugation at 8,500 × *g* for 20 min at 4 °C. Cells were then suspended in lysis buffer and sonicated using an Omni Sonicator Ruptor 400 (2 x 6 min. at 50% power). The lysed cell suspensions were centrifuged at 13,500 × *g* for 1 h at 4 °C. Soluble extract was obtained from supernatant and purified using amylose resin (NEB). The purified protein was frozen at -80 °C in in 20 mM Tris (pH 7.5), 200 mM NaCl, 10 mM maltose, and 10% glycerol. Cofactor F_{420} was purified from M. *smegmatis* mc24517 following published protocols.[60, 61] F420–dependent glucose-6-phosphate dehydrogenase (FGD) was expressed and purified as described earlier.[41]

Nitroreductase enzymatic assay

The nitroreductase enzyme assay was performed by monitoring oxidation of $F_{420}H_2$ spectrophotometrically using fluorescence (Ex/Em 420/470 nm) as previously described.[41, 62] $F_{420}H_2$ was first prepared by overnight reduction of F_{420} with 10 μM FGD and 10 mM glucose-6-phosphate in 20 mM Tris-HCl (pH 7.5) under anaerobic conditions. FGD was removed by spin filtration in a 0.5-mL 10K molecular-weights cutoff (MWCO) spin filter (Millipore), and F420H2 was used within 1 h of FGD being removed. The reaction was initiated at room temperature by adding 0.1–1 μM of Ddn enzyme to the assay mixture containing 25 μM of $F_{420}H_2$ and 0-300 μM of substrate in 200 mM Tris-HCl (pH 7.5), 0.1 % Triton X-100. Control reactions without Ddn and without substrate were also performed. Specific enzyme activity of $F_{420}H_2$ oxidation was calculated using a standard curve of F_{420}. To determine the correlation between k_{cat}/K_m values and its whole cell potency (MIC), Pearson's r-coefficient and statistical significance (*p*) were calculated using GraphPad Prism 9 software (San Diego, CA, USA).

***In vivo* pharmacokinetic study**

The mouse pharmacokinetic study was conducted by WuXi AppTec Co., Ltd. (Shanghai). The experimental procedures were approved by the Institutional Animal Care and Use Committee of WuXi AppTec Co., Ltd. (Protocol number PK01-001-2019v1.0). Compounds were administered to CD-1 male mice via oral (PO) and intravenous (IV) routes, in 20 mg/kg and 5 mg/kg respectively. Compounds **9**, **12**, **14**, **73** and **74** were formulated in 10% DMSO and 90% PEG400, whereas **47** was in a solution of 10% DMSO/40% PEG400/20% cremophor in water. Plasma samples were taken at different time points (IV: 0.083, 0.25, 0.5, 1, 2, 4, 8 and 24 h; PO: 0.25, 0.5, 1, 2, 4, 8 and 24 h). Briefly, 30 μL of blood was taken via submandibular or saphenous vein for the first several time points whereas blood samples at the last time point (24 h) were collected via cardiac puncture when the mouse was under terminal anaesthesia. All blood samples were transferred into pre-chilled microcentrifuge tubes containing 2 μL of 0.5 M of K_2-EDTA as anti-coagulant and were centrifuged at 7,000 rpm, 4 °C for 10 min. Plasma was then collected, frozen over dry ice, and stored at -70 °C until LC-MS/MS analysis. To process the samples prior to analysis, an aliquot of 5 μL was quenched with 300 μL of acetonitrile containing internal standards (labetalol, tolbutamide, verapamil, dexamethasone, glyburide and celecoxib, 100 ng/mL for each). The mixture was vortex-mixed and centrifuged for 15 min at 4,000 rpm, 4 °C. Supernatant (50 μL) was transferred to 96-well plate and centrifuged again for 5 min at 4,000 rpm, 4 °C before injecting to LC-MS/MS. Calibration curve was prepared for quantitation. Mobile phase was 0.1% formic acid & 2 mM ammonium formate in water/acetonitrile (v:v, 95:5) (solvent A) and 0.1% formic acid & 2 mM ammonium formate in acetonitrile/water (v:v, 95:5) (solvent B). LC-MS/MS condition: column ACQUITY UPLC HSS T3 1.8 μm 2.1 × 50 mm; column temperature: 60 °C; flow: 0.6 mL/min; gradient timetable: 0.00 min, 10% B; 1.20 min, 90% B; 1.40 min, 90% B; 1.41 min, 10% B; 1.50 min, 10 % B. Pharmacokinetic data were calculated using Phoenix WinNonlin 6.3 (Certara, Princeton, USA).

In vivo acute TB mouse study

The experimental procedures for acute TB mouse efficacy study were approved by the Animal Care Policies of the University of Illinois at Chicago (ACC Number: 18-135). Female BALB/c mice weighing 21–23 g were infected with *M. tuberculosis* by aerosol. Compounds were formulated in 5% DMSO and 10% hydroxypropyl-β-cyclodextrin prior to administration. The *in vivo* efficacy study was performed according to a published method.[63] At day 10 post-infection, each compound was given orally in 200 µL at different doses (12.5, 25 and 50 mg/kg). The treatment was continued for 3 weeks, 5 days a week. Each treated group composed of 7 mice. Pretomanid **4** was used as the comparator and was dosed at 20 mg/kg. Rifampicin (15 mg/kg) was used as a positive control. The mice were humanely killed after 31 days and the lungs were removed, homogenized and diluted in HBSS before plated onto 7H11 agar. Efficacy results are presented as colony forming unit (CFU) and was plotted using GraphPad Prism 9 (San Diego, CA, USA). Statistical analysis was evaluated by a one-way analysis of variance (ordinary one-way ANOVA), followed by a Dunnett's multiple comparison test to compare the differences between untreated and experiment groups. Results were considered statistically significant at 95% confidence level.

T. cruzi image-based assay

Compounds were screened against *T. cruzi* intracellular amastigotes using an established image-based assay as described previously.[37, 57] Briefly, 3T3 fibroblasts (ATCC CCL92) were infected with *T. cruzi* Tulahuen strain parasites at a multiplicity of 5:1. Compounds, pre diluted in milli-Q H2O, were added to wells to give final assay concentrations ranging in serial log dilutions from 73.3 or 36.6 µM, to $1.8x10^{-4}$ µM or $9x10^{-5}$ µM, respectively. Plates were incubated for 48 h before fixing infected cells with 4% paraformaldehyde containing Hoechst 3348, followed by staining with HCS CellMask™ green (ThermoFisher Scientific). Images were taken on a Phenix high-content cell imager (PerkinElmer). All

experiments were performed over two biological replicates. IC_{50} and CC_{50} values were calculated in GraphPad Prism 9 (San Diego, CA, USA), using a sigmoidal dose-response analysis, with variable slope.

In vivo bioluminescence study of experimental acute stage *Trypanosoma cruzi* infections

All animal work was performed under UK Home Office license PPL P9AEE04E4 and approved by the London School of Hygiene and Tropical Medicine Animal Welfare and Ethical Review Board (AWERB). All protocols and procedures were conducted in accordance with the UK Animals (Scientific Procedures) Act 1986. The study was performed with a slight modification as previously described.[64] Female BALB/c mice (n=3/group) were purchased from Charles River (UK) and maintained under specific pathogen-free conditions in individually ventilated cages. They experienced a 12-hour light/dark cycle and had access to food and water *ad libitum*. Bioluminescent *T. cruzi* CL Brener parasites were generated by genetic transformation with the construct pTRIX2-RE9h.[65] Mice were injected i.p. with 10^3 bloodstream form trypomastigotes (in 0.2 mL in D-PBS) obtained from infected SCID mice. Compounds **73** and **74** were formulated in 5% DMSO and 10% hydroxypropyl-β-cyclodextrin at 5 mg/mL and prepared daily before administration. Benznidazole **1** was formulated in an aqueous suspension vehicle containing 0.5% (w/v) hydroxypropyl methylcellulose and 0.4% (v/v) Tween 80 at 10 mg/mL on the first day of treatment and left at 4 °C until needed. When infections had reached the acute stage at day 14 post-infection, each compound was administered by oral gavage (adjusted by weight), and vehicle only was administered to control mice (negative control), for 5 days at 50 mg/kg for **73** and **74** and 100 mg/kg for **1** (positive control). Compound **73** was given once a day (UID), while **74** was given twice daily (BID) due to its lower half-life (Table 8). For bioluminescence imaging, mice were injected with 150 mg/kg d-luciferin i.p., then anaesthetized using 2.5% (v/v) gaseous isoflurane in oxygen for 2-3 min. Mice were placed in an IVIS Spectrum system (Caliper Life Science) and images acquired 10-20 min after d-luciferin administration using Living Image® 4.3. Exposure times varied from 10 secs to 5min, depending on signal intensity. After imaging, mice were returned to cages. To estimate parasite burden,

regions of interest (ROIs) were drawn using Living Image® 4.3 to quantify bioluminescence expressed as total flux (photons/second; p/s). The detection threshold was established from uninfected mice.

Corresponding Author Information

*E-mail: m.blaskovich@uq.edu.au Telephone: +61 7 3346 2994

*E-mail: ang.cheewei@monash.edu Telephone: +60 3 5514 6112

Author Contributions

The manuscript was written through contributions of all authors. All authors have given approval to the final version of the manuscript.

Acknowledgement

We are thankful to the support from the University of Queensland, Australian National University, University of Illinois at Chicago, London School of Hygiene & Tropical Medicine, and Griffith University for providing facilities. We also thank Angie Jarrad for helpful discussions at the early stage of this work. CWA was supported by an Australian Government Research Training Program scholarship. MLS was the recipient of a Griffith University Post-doctoral Fellowship (GUPF) award. MAB was supported in part by Wellcome Trust Strategic Award 104797/Z/14/Z. MAC is a NHMRC Principal Research Fellow (APP1059354) and holds a fractional professorial research fellow appointment at The University of Queensland, with his remaining time as CEO of Inflazome Ltd, a company developing drugs to address clinical unmet needs in inflammatory disease. JMK was supported by UK Medical Research Council (MRC) Grant MR/T015969/1.

Abbreviations Used

CD, Chagas diseases; CL, total systemic clearance; C_{max}, maximum concentration; CV, cyclic voltammetry; Ddn, deazaflavin-dependent nitroreductase; E', formal potential; HAT, human African

trypanosomiasis; MIC, Minimum Inhibitory Concentration; ND, not determined; NTD, neglected tropical diseases; NTR, nitroreductase; T_{max}, time to reach maximum concentration; TPP, target product profiles; VL, visceral leishmaniasis; V_{ss}, steady state volume of distribution

Ancillary Information

Supporting Information

Molecular formula strings (CSV)

Figure S1. Chemical structures of nitroimidazopyrazinones **7–77**.

Figure S2. Chemical structures of nitroimidazopyrazines **78–90**.

Figure S3. Cyclic voltammogram of (a) 1 mM tested compounds (metronidazole, pretomanid **4** and compound **9**) in DMSO containing 0.1M tetrabutylammonium hexafluorophosphate (TBAHFP), with sweep rate at 200 mV/s. (b) Compound **9** at different sweep rates (50, 100, 200, 500, 1000 and 2000 mV/s).

Table S1. Average body weight of mice at day 10 (starting of treatment) and day 31 (end of treatment) for *M. tuberculosis* infection model.

Figure S4. CFU count data in the lungs of infected mice treated with rifampicin.

Scheme S1. General reaction scheme of nitroimidazopyrazinones.

Figure S5. HPLC traces of compounds (a) **9**, (b) **14**, (c) **73** and (d) **74**.

^{1}H and ^{13}C NMR spectra of nitroimidazoimidazolone **92** and nitroimidazopyrimidinone **93**.

References

1. *WHO Global tuberculosis report 2021*; Geneva, 2021.
2. Katsuno, K.; Burrows, J. N.; Duncan, K.; van Huijsduijnen, R. H.; Kaneko, T.; Kita, K.; Mowbray, C. E.; Schmatz, D.; Warner, P.; Slingsby, B. T., Hit and lead criteria in drug discovery for infectious diseases of the developing world. *Nat. Rev. Drug Discov.* **2015,** *14* (11), 751-758.
3. *Target Regimen Profiles for TB Treatment (WHO/HTM/TB/2016.16)*; World Health Organisation Geneva, 2016.
4. Bhutta, Z. A.; Sommerfeld, J.; Lassi, Z. S.; Salam, R. A.; Das, J. K., Global burden, distribution, and interventions for infectious diseases of poverty. *Infect. Dis. Poverty.* **2014,** *3*, 21.
5. Lee, B. Y.; Bacon, K. M.; Bottazzi, M. E.; Hotez, P. J., Global economic burden of Chagas disease: a computational simulation model. *Lancet Infect. Dis.* **2013,** *13* (4), 342-348.
6. Chagas disease (also known as American trypanosomiasis). https://www.who.int/news-room/fact-sheets/detail/chagas-disease-(american-trypanosomiasis) (accessed Accessed July 11, 2021).
7. Pérez-Molina, J. A.; Molina, I., Chagas disease. *Lancet* **2018,** *391* (10115), 82-94.
8. Lidani, K. C. F.; Andrade, F. A.; Bavia, L.; Damasceno, F. S.; Beltrame, M. H.; Messias-Reason, I. J.; Sandri, T. L., Chagas disease: from discovery to a worldwide health problem. *Front Public Health* **2019,** *7*, 166.
9. Castro, J. A.; de Mecca, M. M.; Bartel, L. C., Toxic side effects of drugs used to treat Chagas' disease (American trypanosomiasis). *Hum. Exp. Toxicol.* **2006,** *25* (8), 471-479.
10. Target product profile for Chagas disease. https://dndi.org/diseases/chagas/target-product-profile/ (accessed Accessed July 2, 2021).
11. Martín-Escolano, J.; Marín, C.; Rosales, M. J.; Tsaousis, A. D.; Medina-Carmona, E.; Martín-Escolano, R., An updated view of the *Trypanosoma cruzi* life cycle: intervention points for an effective treatment. *ACS Infect. Dis.* **2022,** *8* (6), 1107-1115.

12. Mazzeti, A. L.; Diniz, L. d. F.; Gonçalves, K. R.; WonDollinger, R. S.; Assíria, T.; Ribeiro, I.; Bahia, M. T., Synergic effect of allopurinol in combination with nitroheterocyclic compounds against *Trypanosoma cruzi*. *Antimicrob. Agents Chemother.* **2019,** *63* (6), e02264-18.

13. Torrico, F.; Gascón, J.; Barreira, F.; Blum, B.; Almeida, I. C.; Alonso-Vega, C.; Barboza, T.; Bilbe, G.; Correia, E.; Garcia, W.; Ortiz, L.; Parrado, R.; Ramirez, J. C.; Ribeiro, I.; Strub-Wourgaft, N.; Vaillant, M.; Sosa-Estani, S.; Arteaga, R.; de la Barra, A.; Camacho Borja, J.; Martinez, I.; Fernandes, J.; Garcia, L.; Lozano, D.; Palacios, A.; Schijman, A.; Pinazo, M. J.; Pinto, J.; Rojas, G.; Estevao, I.; Ortega-Rodriguez, U.; Mendes, M. T.; Schuck, E.; Hata, K.; Maki, N.; Asada, M., New regimens of benznidazole monotherapy and in combination with fosravuconazole for treatment of Chagas disease (BENDITA): a phase 2, double-blind, randomised trial. *Lancet Infect. Dis.* **2021,** *21* (8), 1129-1140.

14. Grzelak, E. M.; Choules, M. P.; Gao, W.; Cai, G.; Wan, B.; Wang, Y.; McAlpine, J. B.; Cheng, J.; Jin, Y.; Lee, H.; Suh, J.-W.; Pauli, G. F.; Franzblau, S. G.; Jaki, B. U.; Cho, S., Strategies in anti-*Mycobacterium tuberculosis* drug discovery based on phenotypic screening. *J. Antibiot.* **2019,** *72* (10), 719-728.

15. Field, M. C.; Horn, D.; Fairlamb, A. H.; Ferguson, M. A. J.; Gray, D. W.; Read, K. D.; De Rycker, M.; Torrie, L. S.; Wyatt, P. G.; Wyllie, S.; Gilbert, I. H., Anti-trypanosomatid drug discovery: an ongoing challenge and a continuing need. *Nat. Rev. Microbiol.* **2017,** *15* (4), 217-231.

16. Torreele, E.; Bourdin Trunz, B.; Tweats, D.; Kaiser, M.; Brun, R.; Mazue, G.; Bray, M. A.; Pecoul, B., Fexinidazole - a new oral nitroimidazole drug candidate entering clinical development for the treatment of sleeping sickness. *PLoS Negl. Trop. Dis.* **2010,** *4* (12), e923.

17. Bahia, M. T.; de Andrade, I. M.; Martins, T. A. F.; do Nascimento, Á. F. d. S.; Diniz, L. d. F.; Caldas, I. S.; Talvani, A.; Trunz, B. B.; Torreele, E.; Ribeiro, I., Fexinidazole: a potential new drug candidate for Chagas disease. *PLoS Negl. Trop. Dis.* **2012,** *6* (11), e1870.

18. Cole, S. T., Inhibiting *Mycobacterium tuberculosis* within and without. *Philosophical Transactions of the Royal Society B: Biological Sciences* **2016,** *371* (1707), 20150506.

19. Patterson, S.; Wyllie, S.; Norval, S.; Stojanovski, L.; Simeons, F. R. C.; Auer, J. L.; Osuna-Cabello, M.; Read, K. D.; Fairlamb, A. H., The anti-tubercular drug delamanid as a potential oral treatment for visceral leishmaniasis. *eLife* **2016,** *5*, e09744.

20. Patterson, S.; Wyllie, S.; Stojanovski, L.; Perry, M. R.; Simeons, F. R.; Norval, S.; Osuna-Cabello, M.; De Rycker, M.; Read, K. D.; Fairlamb, A. H., The *R* enantiomer of the antitubercular drug PA-824 as a potential oral treatment for visceral leishmaniasis. *Antimicrob. Agents Chemother.* **2013,** *57* (10), 4699-4706.

21. Thompson, A. M.; Marshall, A. J.; Maes, L.; Yarlett, N.; Bacchi, C. J.; Gaukel, E.; Wring, S. A.; Launay, D.; Braillard, S.; Chatelain, E.; Mowbray, C. E.; Denny, W. A., Assessment of a pretomanid analogue library for African trypanosomiasis: Hit-to-lead studies on 6-substituted 2-nitro-6,7-dihydro-5*H*-imidazo[2,1-*b*][1,3]thiazine 8-oxides. *Bioorg. Med. Chem. Lett.* **2018,** *28* (2), 207-213.

22. Thompson, A. M.; O'Connor, P. D.; Marshall, A. J.; Francisco, A. F.; Kelly, J. M.; Riley, J.; Read, K. D.; Perez, C. J.; Cornwall, S.; Thompson, R. C. A.; Keenan, M.; White, K. L.; Charman, S. A.; Zulfiqar, B.; Sykes, M. L.; Avery, V. M.; Chatelain, E.; Denny, W. A., Re-evaluating pretomanid analogues for Chagas disease: Hit-to-lead studies reveal both *in vitro* and *in vivo* trypanocidal efficacy. *Eur. J. Med. Chem.* **2020,** *207*, 112849.

23. Ang, C. W.; Jarrad, A. M.; Cooper, M. A.; Blaskovich, M. A. T., Nitroimidazoles: molecular fireworks that combat a broad spectrum of infectious diseases. *J. Med. Chem.* **2017,** *60* (18), 7636-7657.

24. Mukherjee, T.; Boshoff, H., Nitroimidazoles for the treatment of TB: past, present and future. *Future Med. Chem.* **2011,** *3* (11), 1427-1454.

25. Stover, C. K.; Warrener, P.; VanDevanter, D. R.; Sherman, D. R.; Arain, T. M.; Langhorne, M. H.; Anderson, S. W.; Towell, J. A.; Yuan, Y.; McMurray, D. N.; Kreiswirth, B. N.; Barry, C. E.; Baker, W. R., A small-molecule nitroimidazopyran drug candidate for the treatment of tuberculosis. *Nature* **2000,** *405* (6789), 962-966.

26. Singh, R.; Manjunatha, U.; Boshoff, H. I.; Ha, Y. H.; Niyomrattanakit, P.; Ledwidge, R.; Dowd, C. S.; Lee, I. Y.; Kim, P.; Zhang, L.; Kang, S.; Keller, T. H.; Jiricek, J.; Barry, C. E., 3rd, PA-824 kills nonreplicating *Mycobacterium tuberculosis* by intracellular NO release. *Science* **2008,** *322* (5906), 1392-1395.

27. Matsumoto, M.; Hashizume, H.; Tomishige, T.; Kawasaki, M.; Tsubouchi, H.; Sasaki, H.; Shimokawa, Y.; Komatsu, M., OPC-67683, a nitro-dihydro-imidazooxazole derivative with promising action against tuberculosis *in vitro* and in mice. *PLoS Med.* **2006,** *3* (11), e466.

28. Manjunatha, U. H.; Boshoff, H.; Dowd, C. S.; Zhang, L.; Albert, T. J.; Norton, J. E.; Daniels, L.; Dick, T.; Pang, S. S.; Barry, C. E., 3rd, Identification of a nitroimidazo-oxazine-specific protein involved in PA-824 resistance in *Mycobacterium tuberculosis*. *Proc. Natl. Acad. Sci. U.S.A* **2006,** *103* (2), 431-436.

29. Cellitti, S. E.; Shaffer, J.; Jones, D. H.; Mukherjee, T.; Gurumurthy, M.; Bursulaya, B.; Boshoff, H. I.; Choi, I.; Nayyar, A.; Lee, Y. S.; Cherian, J.; Niyomrattanakit, P.; Dick, T.; Manjunatha, U. H.; Barry, C. E., 3rd; Spraggon, G.; Geierstanger, B. H., Structure of Ddn, the deazaflavin-

dependent nitroreductase from *Mycobacterium tuberculosis* involved in bioreductive activation of PA-824. *Structure* **2012,** *20* (1), 101-112.

30. Hayashi, M.; Nishiyama, A.; Kitamoto, R.; Tateishi, Y.; Osada-Oka, M.; Nishiuchi, Y.; Kaboso, S. A.; Chen, X.; Fujiwara, M.; Inoue, Y.; Kawano, Y.; Kawasaki, M.; Abe, T.; Sato, T.; Kaneko, K.; Itoh, K.; Matsumoto, S.; Matsumoto, M., Adduct formation of delamanid with NAD in *Mycobacteria*. *Antimicrob. Agents Chemother.* **2020,** *64* (5), e01755-19.

31. Wyllie, S.; Roberts, A. J.; Norval, S.; Patterson, S.; Foth, B. J.; Berriman, M.; Read, K. D.; Fairlamb, A. H., Activation of bicyclic nitro-drugs by a novel nitroreductase (NTR2) in Leishmania. *PLoS Pathog.* **2016,** *12* (11), e1005971.

32. Wyllie, S.; Patterson, S.; Stojanovski, L.; Simeons, F. R. C.; Norval, S.; Kime, R.; Read, K. D.; Fairlamb, A. H., The anti-trypanosome drug fexinidazole shows potential for treating visceral leishmaniasis. *Sci. Transl. Med.* **2012,** *4* (119), 119re1.

33. Dickie, E. A.; Giordani, F.; Gould, M. K.; Mäser, P.; Burri, C.; Mottram, J. C.; Rao, S. P. S.; Barrett, M. P., New drugs for human African trypanosomiasis: a twenty first century success story. *Trop. Med. Infect. Dis.* **2020,** *5* (1), 29.

34. Jarrad, A. M.; Ang, C. W.; Debnath, A.; Hahn, H. J.; Woods, K.; Tan, L.; Sykes, M. L.; Jones, A. J.; Pelingon, R.; Butler, M. S.; Avery, V. M.; West, N. P.; Karoli, T.; Blaskovich, M. A. T.; Cooper, M. A., Design, synthesis, and biological evaluation of 2-nitroimidazopyrazin-one/-es with antitubercular and antiparasitic activity. *J. Med. Chem.* **2018,** *61* (24), 11349-11371.

35. Kim, P.; Zhang, L.; Manjunatha, U. H.; Singh, R.; Patel, S.; Jiricek, J.; Keller, T. H.; Boshoff, H. I.; Barry, C. E.; Dowd, C. S., Structure−activity relationships of antitubercular nitroimidazoles. 1. Structural features associated with aerobic and anaerobic activities of 4- and 5-nitroimidazoles. *J. Med. Chem.* **2009,** *52* (5), 1317-1328.

36. Bollo, S.; Núñez-Vergara, L. J.; Squella, J. A., Cyclic voltammetric determination of free radical species from nitroimidazopyran: a new antituberculosis agent. *J. Electroanal. Chem.* **2004,** *562* (1), 9-14.

37. Ang, C. W.; Tan, L.; Sykes, M. L.; AbuGharbiyeh, N.; Debnath, A.; Reid, J. C.; West, N. P.; Avery, V. M.; Cooper, M. A.; Blaskovich, M. A. T., Antitubercular and antiparasitic 2-nitroimidazopyrazinones with improved potency and solubility. *J. Med. Chem.* **2020,** *63* (24), 15726-15751.

38. Baloni, P.; Padiadpu, J.; Singh, A.; Gupta, K. R.; Chandra, N., Identifying feasible metabolic routes in *Mycobacterium smegmatis* and possible alterations under diverse nutrient conditions. *BMC Microbiol.* **2014,** *14* (1), 276.

39. Lelovic, N.; Mitachi, K.; Yang, J.; Lemieux, M. R.; Ji, Y.; Kurosu, M., Application of *Mycobacterium smegmatis* as a surrogate to evaluate drug leads against *Mycobacterium tuberculosis*. *J. Antibiot.* **2020,** *73* (11), 780-789.

40. Malhotra, S.; Vedithi, S. C.; Blundell, T. L., Decoding the similarities and differences among mycobacterial species. *PLoS Negl. Trop. Dis.* **2017,** *11* (8), e0005883.

41. Lee, B. M.; Harold, L. K.; Almeida, D. V.; Afriat-Jurnou, L.; Aung, H. L.; Forde, B. M.; Hards, K.; Pidot, S. J.; Ahmed, F. H.; Mohamed, A. E.; Taylor, M. C.; West, N. P.; Stinear, T. P.; Greening, C.; Beatson, S. A.; Nuermberger, E. L.; Cook, G. M.; Jackson, C. J., Predicting nitroimidazole antibiotic resistance mutations in *Mycobacterium tuberculosis* with protein engineering. *PLoS Pathog.* **2020,** *16* (2), e1008287.

42. Jena, L.; Kashikar, S.; Kumar, S.; Harinath, B., Comparative proteomic analysis of *Mycobacterium tuberculosis* strain H37Rv versus H37Ra. *Int. J. Mycobact* **2013,** *2* (4), 220-226.

43. Zheng, H.; Lu, L.; Wang, B.; Pu, S.; Zhang, X.; Zhu, G.; Shi, W.; Zhang, L.; Wang, H.; Wang, S.; Zhao, G.; Zhang, Y., Genetic basis of virulence attenuation revealed by comparative genomic analysis of *Mycobacterium tuberculosis* strain H37Ra versus H37Rv. *PloS One* **2008,** *3* (6), e2375.

44. Pinto, S. M.; Verma, R.; Advani, J.; Chatterjee, O.; Patil, A. H.; Kapoor, S.; Subbannayya, Y.; Raja, R.; Gandotra, S.; Prasad, T. S. K., Integrated multi-omic analysis of *Mycobacterium tuberculosis* H37Ra redefines virulence attributes. *Front. Microbiol.* **2018,** *9* (1314).

45. Rice, A. M.; Long, Y.; King, S. B., Nitroaromatic antibiotics as nitrogen oxide sources. *Biomolecules* **2021,** *11* (2), 267.

46. Kizaka-Kondoh, S.; Konse-Nagasawa, H., Significance of nitroimidazole compounds and hypoxia-inducible factor-1 for imaging tumor hypoxia. *Cancer Sci.* **2009,** *100* (8), 1366-1373.

47. Wirtanen, T.; Rodrigo, E.; Waldvogel, S. R., Recent advances in the electrochemical reduction of substrates involving N−O bonds. *Adv. Synth. Catal.* **2020,** *362* (11), 2088-2101.

48. Gurumurthy, M.; Mukherjee, T.; Dowd, C. S.; Singh, R.; Niyomrattanakit, P.; Tay, J. A.; Nayyar, A.; Lee, Y. S.; Cherian, J.; Boshoff, H. I.; Dick, T.; Barry, C. E., 3rd; Manjunatha, U. H., Substrate specificity of the deazaflavin-dependent nitroreductase from *Mycobacterium tuberculosis* responsible for the bioreductive activation of bicyclic nitroimidazoles. *Febs J.* **2012,** *279* (1), 113-125.

49. Kim, P.; Kang, S.; Boshoff, H. I.; Jiricek, J.; Collins, M.; Singh, R.; Manjunatha, U. H.; Niyomrattanakit, P.; Zhang, L.; Goodwin, M.; Dick, T.; Keller, T. H.; Dowd, C. S.; Barry, C. E., Structure−activity relationships of antitubercular nitroimidazoles. 2. Determinants of aerobic activity and quantitative structure−activity relationships. *J. Med. Chem.* **2009,** *52* (5), 1329-1344.

50. Palmer, B. D.; Thompson, A. M.; Sutherland, H. S.; Blaser, A.; Kmentova, I.; Franzblau, S. G.; Wan, B.; Wang, Y.; Ma, Z.; Denny, W. A., Synthesis and structure−activity studies of biphenyl

analogues of the tuberculosis drug (6*S*)-2-nitro-6-{[4-(trifluoromethoxy)benzyl]oxy}-6,7-dihydro-5*H*-imidazo[2,1-*b*][1,3]oxazine (PA-824). *J. Med. Chem.* **2010,** *53* (1), 282-294.

51. Palmer, B. D.; Sutherland, H. S.; Blaser, A.; Kmentova, I.; Franzblau, S. G.; Wan, B.; Wang, Y.; Ma, Z.; Denny, W. A.; Thompson, A. M., Synthesis and structure–activity relationships for extended side chain analogues of the antitubercular drug (6*S*)-2-nitro-6-{[4-(trifluoromethoxy)benzyl]oxy}-6,7-dihydro-5*H*-imidazo[2,1-*b*][1,3]oxazine (PA-824). *J. Med. Chem.* **2015,** *58* (7), 3036-3059.

52. Thompson, A. M.; Blaser, A.; Anderson, R. F.; Shinde, S. S.; Franzblau, S. G.; Ma, Z.; Denny, W. A.; Palmer, B. D., Synthesis, reduction potentials, and antitubercular activity of ring A/B analogues of the bioreductive drug (6*S*)-2-nitro-6-{[4-(trifluoromethoxy)benzyl]oxy}-6,7-dihydro-5*H*-imidazo[2,1-*b*][1,3]oxazine (PA-824). *J. Med. Chem.* **2009,** *52* (3), 637-645.

53. Thompson, A. M.; O'Connor, P. D.; Marshall, A. J.; Yardley, V.; Maes, L.; Gupta, S.; Launay, D.; Braillard, S.; Chatelain, E.; Franzblau, S. G.; Wan, B.; Wang, Y.; Ma, Z.; Cooper, C. B.; Denny, W. A., 7-Substituted 2-nitro-5,6-dihydroimidazo[2,1-*b*][1,3]oxazines: novel antitubercular agents lead to a new preclinical candidate for visceral leishmaniasis. *J. Med. Chem.* **2017,** *60* (10), 4212-4233.

54. Montalbetti, C. A. G. N.; Falque, V. M., Amide bond formation and peptide coupling. *Tetrahedron* **2005,** *61*, 10827-10852.

55. Lakshminarayana, S. B.; Boshoff, H. I. M.; Cherian, J.; Ravindran, S.; Goh, A.; Jiricek, J.; Nanjundappa, M.; Nayyar, A.; Gurumurthy, M.; Singh, R.; Dick, T.; Blasco, F.; Barry, C. E., III; Ho, P. C.; Manjunatha, U. H., Pharmacokinetics-pharmacodynamics analysis of bicyclic 4-nitroimidazole analogs in a murine model of tuberculosis. *PloS One* **2014,** *9* (8), e105222.

56. Moraes, C. B.; Giardini, M. A.; Kim, H.; Franco, C. H.; Araujo-Junior, A. M.; Schenkman, S.; Chatelain, E.; Freitas-Junior, L. H., Nitroheterocyclic compounds are more efficacious than CYP51

inhibitors against *Trypanosoma cruzi*: implications for Chagas disease drug discovery and development. *Sci. Rep.* **2014,** *4* (1), 4703.

57. Sykes, M. L.; Avery, V. M., 3-Pyridyl inhibitors with novel activity against *Trypanosoma cruzi* reveal *in vitro* profiles can aid prediction of putative cytochrome P450 inhibition. *Sci. Rep.* **2018,** *8* (1), 4901.

58. Chatelain, E., Chagas disease drug discovery: toward a new era. *J. Biomol. Screen* **2015,** *20* (1), 22-35.

59. Aragaw, W. W.; Lee, B. M.; Yang, X.; Zimmerman, M. D.; Gengenbacher, M.; Dartois, V.; Chui, W.-K.; Jackson, C. J.; Dick, T., Potency boost of a *Mycobacterium tuberculosis* dihydrofolate reductase inhibitor by multienzyme $F_{420}H_2$-dependent reduction. *Proc. Natl. Acad. Sci. U.S.A* **2021,** *118* (25), e2025172118.

60. Bashiri, G.; Rehan, A. M.; Greenwood, D. R.; Dickson, J. M. J.; Baker, E. N., Metabolic engineering of cofactor F_{420} production in *Mycobacterium smegmatis*. *PloS One* **2011,** *5* (12), e15803.

61. Isabelle, D.; Simpson, D. R.; Daniels, L., Large-scale production of coenzyme F_{420}-5,6 by using *Mycobacterium smegmatis.* *Appl. Environ. Microbiol.* **2002,** *68* (11), 5750-5755.

62. Ahmed, F. H.; Carr, P. D.; Lee, B. M.; Afriat-Jurnou, L.; Mohamed, A. E.; Hong, N.-S.; Flanagan, J.; Taylor, M. C.; Greening, C.; Jackson, C. J., Sequence–structure–function classification of a catalytically diverse oxidoreductase superfamily in mycobacteria. *J. Mol. Biol.* **2015,** *427* (22), 3554-3571.

63. Falzari, K.; Zhu, Z.; Pan, D.; Liu, H.; Hongmanee, P.; Franzblau, S. G., *In vitro* and *in vivo* activities of macrolide derivatives against *Mycobacterium tuberculosis*. *Antimicrob. Agents Chemother.* **2005,** *49* (4), 1447-1454.

64. Francisco, A. F.; Jayawardhana, S.; Lewis, M. D.; White, K. L.; Shackleford, D. M.; Chen, G.; Saunders, J.; Osuna-Cabello, M.; Read, K. D.; Charman, S. A.; Chatelain, E.; Kelly, J. M., Nitroheterocyclic drugs cure experimental *Trypanosoma cruzi* infections more effectively in the chronic stage than in the acute stage. *Sci. Rep.* **2016,** *6* (1), 35351.

65. Lewis, M. D.; Fortes Francisco, A.; Taylor, M. C.; Burrell-Saward, H.; McLatchie, A. P.; Miles, M. A.; Kelly, J. M., Bioluminescence imaging of chronic *Trypanosoma cruzi* infections reveals tissue-specific parasite dynamics and heart disease in the absence of locally persistent infection. *Cell. Microbiol.* **2014,** *16* (9), 1285-1300.

Table of Contents graphic